

# The Dynamic Response of Vegetation Water Use Efficiency to Wildfire Disturbances in the Northern Hemisphere

Huipeng Xi<sup>1</sup>, Qunming Wang<sup>1,\*</sup>, Peter M. Atkinson<sup>2,3</sup>

<sup>1</sup>College of Surveying and Geo-Informatics, Tongji University, 1239 Siping Road, Shanghai, 200092, China.

<sup>2</sup>Faculty of Science and Technology, Lancaster University, Lancaster LA1 4YR, UK.

<sup>3</sup>Geography and Environment, University of Southampton, Highfield, Southampton SO17 1BJ, UK.

*Corresponding author: Qunming Wang (wqm11111@126.com).*

## Abstract

Vegetation water use efficiency (WUE) serves as a critical indicator reflecting the interactions between ecosystem carbon and water cycles. However, rapid warming in the Northern Hemisphere and increasing wildfire activities have introduced significant disturbances, and potentially affected the dynamic changes in WUE that occur post-fire. Understanding these impacts is crucial for advancing our knowledge of ecosystem responses to environmental changes. In this research, we focused on analyzing the post-fire trajectories and response mechanisms of WUE during the growing season in the Northern Hemisphere by employing detrended and de-seasonalized WUE data combined with fire intensity derived from the moderate resolution imaging spectroradiometer. Our findings reveal that since 2001, the WUE of vegetation in the northern hemisphere during the growing season exhibited an overall downward trend ( $-0.016 \text{ g C m}^{-2} \text{ mm}^{-1} \text{ yr}^{-1}$ ), with a pronounced turning point observed around 2011, which may be related to large-scale climate anomalies, such as the strong La Niña event. Within five years after fire, 74.2% of  $\Delta\text{WUE}$  (defined as post-fire WUE minus pre-fire WUE) values fell within the range of  $-0.5$  to  $0.5 \text{ g C m}^{-2} \text{ mm}^{-1}$  and showing a clear bias toward negative values, indicating that fire disturbances tended to produce adverse impacts on WUE. Notably, coniferous forests exhibited increasing WUE trends post-fire, whereas broadleaf forests tended to decline, with their trajectories further influenced by climatic zones. Machine

32 learning-based attribution analysis highlighted that the pre-fire levels of WUE was a  
33 key factor influencing post-fire changes in WUE. Additionally, climate variables such  
34 as temperature, vapor pressure deficit, soil moisture, and precipitation also played  
35 important roles, these climatic drivers contributed significantly at local scales. Our  
36 study reveals post-fire trajectories of WUE among different vegetation types and  
37 identifies the primary drivers. These findings provide important insights for  
38 understanding coupled carbon-water cycle responses of northern vegetation to fire  
39 disturbance.

40

41 **Keywords:** Water use efficiency, Fire disturbance, Post-fire vegetation recovery,  
42 Climate change, Northern Hemisphere

43

## 44 **1. Introduction**

45 Water use efficiency (WUE), defined as the ratio of carbon assimilated by plants  
46 to the transpiration water consumed, reflects vegetation growth capacity under  
47 specific water resources conditions and serves as a critical indicator for evaluating the  
48 integrated response of land ecosystems to the carbon, water, and energy cycles ([Ito  
49 and Inatomi, 2012](#); [Huang et al., 2015](#); [Yang et al., 2020](#)). Consequently, dynamic  
50 changes in WUE and its control mechanisms have been a focal area of global change  
51 ecology research. Early studies demonstrated that elevated CO<sub>2</sub> concentrations under  
52 free-air CO<sub>2</sub> enrichment conditions enhance photosynthesis in both C3 and C4  
53 vegetation while reducing stomatal conductance, thereby, improving WUE ([Wand et  
54 al., 1999](#); [Bernacchi et al., 2007](#)). In recent years, large-scale studies using remote  
55 sensing technology have further revealed that WUE shows a significant increasing  
56 trend in regions with vegetative greening ([Xue et al., 2022](#); [Hu et al., 2024](#)), offering  
57 new perspectives on understanding vegetation-water resource relationships. However,  
58 under drought stress conditions, particularly in environments characterized by high  
59 vapor pressure deficit (VPD) and low soil moisture, vegetation limits photosynthesis  
60 and transpiration processes through stomatal regulation mechanisms, potentially

61 limiting further global-scale WUE increases to an asymptote, that is, a saturation level  
62 (Li et al., 2023). Recent studies have further indicated that the spatiotemporal  
63 variations in WUE and their drivers exhibit spatial heterogeneity and high sensitivity  
64 to extreme climate events (Liu et al., 2024). Although some studies have examined  
65 the response of WUE to drought stress, research focusing solely on fire disturbances,  
66 particularly at large spatial scales, remains limited. In the context of intensified global  
67 climate change, vegetation recovery has become increasingly longer following  
68 extreme fire events in recent years (Lv et al., 2025). Therefore, it is necessary to  
69 investigate post-fire WUE trajectories at large spatial scales and to examine the  
70 mechanisms by which fire disturbances influence WUE.

71 The occurrence of wildfires typically causes severe disruption to the surface  
72 environment, and the overlay of drought stress before and after a fire complicates the  
73 vegetation growth trajectories. Existing research indicates that fires can influence  
74 ecosystem water and carbon cycles on multiple levels. At the biogeochemical level,  
75 fires affect water transport processes directly by regulating plant water demand (Baur  
76 et al., 2024) and altering soil texture (Granged et al., 2011); at the community  
77 structure level, fires drive changes in vegetation cover types (Tyukavina et al., 2022)  
78 and reshape ecosystem resilience (Zheng et al., 2024), indirectly influencing carbon  
79 and water use patterns; at the energy exchange level, fires reconstruct regional surface  
80 energy and water balance by altering surface radiation flux and the evapotranspiration  
81 capacity of vegetation (Liu et al., 2019; Zhao et al., 2024).

82 However, fire characteristics differ markedly between the Northern and Southern  
83 Hemispheres, particularly in terms of fire frequency, area, intensity, and weather  
84 seasons (Jones et al., 2022; Richardson et al., 2022), requiring that regional context  
85 and vegetation types be carefully considered when assessing the impacts of fires on  
86 WUE. Terrestrial ecosystems in the Northern Hemisphere exhibit significant  
87 environmental sensitivity compared to tropical vegetation in the Southern Hemisphere.  
88 Their photosynthesis-transpiration coupling processes are regulated by  
89 multidimensional environmental gradients, encompassing seasonal precipitation  
90 fluctuations, temperature gradients, species differences and elevation effects (Zheng et

91 [al., 2023](#)). Of particular interest is the synergistic interaction between fuel load  
92 heterogeneity and phenological periodicity, which jointly drive the spatiotemporal  
93 pattern formation of wildfires in northern forest regions. On a broader scale, this  
94 interaction shapes the fire type differentiation between North America and Eurasia:  
95 northern forests in North America are dominated by crown fires, while Eurasia  
96 predominantly experiences surface fires ([Rogers et al., 2015](#); [De Groot et al., 2013](#)).  
97 Additionally, compared to wildfire-prone areas in the Southern Hemisphere,  
98 particularly in Australia, the relatively longer fire return intervals in the Northern  
99 Hemisphere have distinct ecological significance, as fires in high-latitude regions are  
100 typically naturally ignited. These temporal characteristics of the fire regime allow  
101 northern hemisphere vegetation to exhibit more complete restoration and succession  
102 processes, providing a unique temporal framework for analyzing vegetation WUE  
103 responses to fire disturbances.

104       Recent years have seen the intensification of Arctic amplification, which has  
105 exacerbated the trend of warming and increased moisture in high-latitude regions,  
106 leading to characteristics such as the expansion of burned areas, increased fire  
107 intensity and prolonged ecological recovery periods in northern forests. A study based  
108 on post-fire carbon stock trajectories showed that the recovery of ecosystem carbon  
109 stocks in northern North American forests exhibited a significant time lag effect, with  
110 recovery periods extending beyond 10 years ([Yu et al., 2023](#)). Despite this, research  
111 on the spatiotemporal evolution of WUE following fire disturbances in northern  
112 regions remains scarce. Understanding the dynamic response mechanisms of WUE  
113 post-fire is crucial for clarifying water-carbon coupling processes in ecosystems under  
114 climate change and for reconstructing regional hydrological cycles.

115       Changes in WUE are revealed as a temporal trend influenced by a combination  
116 of driving factors, including climate and disturbances. Therefore, when analyzing the  
117 isolated effects of disturbances on WUE, it is crucial to remove confounding factors  
118 such as climate change in order to assess the disturbance effects independently. In  
119 previous studies on the impacts of disturbances like fire on vegetation productivity  
120 and resilience, long-term trends and seasonal fluctuations in vegetation were typically

121 removed (Wang et al., 2023; Xu et al., 2024). This methodological approach is highly  
122 relevant for analyzing WUE. However, research focusing on detrended  
123 WUE—defined as the residual variability after removing long-term trends and  
124 seasonal cycles, which captures transient responses to disturbances (e.g., droughts,  
125 fires) and interannual climate extremes—remains limited, highlighting a critical gap  
126 in understanding short-term ecosystem vulnerability.

127 Given the above existing knowledge gaps, we aim to address the following three  
128 questions by integrating de-trended WUE and fire data:

129 1) How has WUE in the Northern Hemisphere changed since the early 21st  
130 century (2001–2021)?

131 2) How does WUE change following fire disturbances?

132 3) What factors influence the evolution of WUE trajectories after fire  
133 disturbances?

134 Through a combination of remote sensing diagnostics and machine  
135 learning-based modeling, we aim to establish a mechanistic framework linking  
136 post-fire vegetation regeneration strategies and hydrological constraints. The findings  
137 will inform adaptive management strategies for balancing carbon sequestration and  
138 water resource sustainability in boreal fire landscapes.

139

## 140 **2. Data and methods**

### 141 **2.1 Overview of the study area**

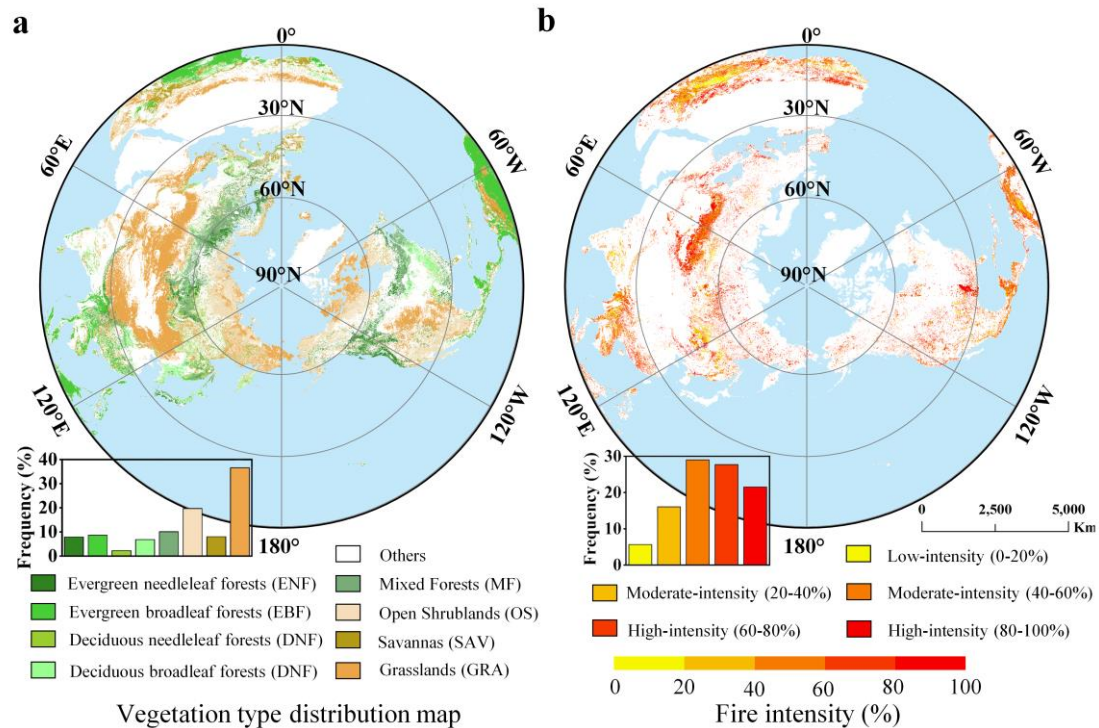
142 The study area is defined within the natural vegetation regions of the Northern  
143 Hemisphere (Fig. 1a), focusing on eight typical vegetation types, and excluding the  
144 interference of agricultural and industrial activities to minimize human impact on the  
145 results. The spatial distribution of vegetation exhibits significant spatial heterogeneity.  
146 Coniferous forests dominate the Siberian and northern Canadian regions (with a  
147 notable proportion north of 55°N), while temperate grasslands occupy a dominant  
148 ecological niche in the Midwest of the United States and Europe, with higher

149 coverage observed in regions between 30-50 °N.

150 We generated a map of wildfire intensity in the Northern Hemisphere since the  
151 21st century. This map was referred to the research of Liu et al. (2019), using an  
152 annual wildfire and vegetation index dataset. Specifically, the intensity is determined  
153 by the ratio of the area of leaf area index (LAI) loss due to fire to the area of the fire  
154 (Equation 1). The results show that high-intensity fire areas (fire intensity > 60%)  
155 account for a significant proportion of the area, mainly distributed in the coniferous  
156 forest belt above 50 °N, while low-intensity fire areas (fire intensity < 20%) represent  
157 a relatively low proportion and are predominantly found in the grassland-forest  
158 transition zone (Fig. 1b).

$$159 \quad \text{Fire intensity} = \frac{\text{Area}_{LAI \text{ loss due to fire}}}{\text{Area}_{Fire}} \times 100\% \quad (1)$$

160 Here,  $\text{Area}_{LAI \text{ loss due to fire}}$  represents the total area within a 0.1 ° grid where a  
161 reduction in LAI due to fire is detected; whereas  $\text{Area}_{Fire}$  represents the fire-affected  
162 area detected within the same grid. Methodologically, we employ a before-and-after  
163 comparison approach to evaluate the impact of fire on vegetation: specifically, within  
164 a three-month time window before and after the fire event, if a significant reduction in  
165 LAI values is observed in 500 m resolution burned pixels, those pixels are classified  
166 as fire-induced LAI loss pixels.



167

168 **Fig. 1.** Land cover and multi-year wildfire intensity distribution characteristics in the study area. a.

169 Spatial distribution of the eight major natural vegetation types, with an inset showing the

170 frequency percentage of each type. b. Map of the average fire intensity from 2001 to 2022, with an

171 inset illustrating the frequency distribution of different wildfire intensity levels.

172

## 173 2.2 Datasets

174 The data used in this study serve three main purposes: estimating WUE,

175 assessing fire intensity, and identifying the environmental factors influencing post-fire

176 WUE trajectories. First, the data used to estimate vegetation WUE come primarily

177 from the PML\_V2 product, which provides gross primary productivity (GPP) and

178 evapotranspiration (ET) data. This product combines a photosynthesis model with a

179 stomatal conductance model and employs the Penman-Monteith equation to estimate

180 GPP and ET. It offers estimates of vegetation water use from 2001 to 2021 at a spatial

181 resolution of 500 m and a temporal resolution of 8 days (Zhang et al., 2019; Ma and

182 Zhang, 2022).

183 Second, we used the monthly 500 m resolution burn product from MCD64A1

184 (Giglio et al., 2021), which effectively records historical wildfire information but is

185 not sensitive to small, isolated fires (Ramo et al., 2021). We estimated wildfire  
 186 intensity and retained pixels where only one fire occurred between 2004 and 2020,  
 187 and the fire intensity was greater than 10%. The land cover type data were obtained  
 188 mainly from MCD12Q1 Version 6.1, which provides global land cover categories  
 189 from 2001 to 2022 at a spatial resolution of 0.05 ° (Friedl and Sulla-Menashe, 2022).  
 190 To minimize potential interference from land cover type changes, we analyzed only  
 191 pixels where no land use change occurred during the fire event.

192 Finally, when evaluating the factors influencing post-fire WUE trajectories, we  
 193 considered environmental characteristics such as climate, soil and fire features.  
 194 Monthly climate data from 2001 to 2022 (with a spatial resolution of 50 km) were  
 195 obtained from the Climate Research Unit (CRU) time-series dataset v.4.08 (Harris et  
 196 al., 2020). Elevation data were sourced from the Shuttle Radar Topography Mission,  
 197 with a spatial resolution of approximately 30 m (Farr et al., 2007). The calculation of  
 198 VPD followed Yao et al. (2023) and was derived from the European Centre for  
 199 Medium-Range Weather Forecasting Reanalysis 5th Generation (ERA5), based on 2  
 200 m air temperature, dew point temperature and elevation (Muñoz Sabater et al., 2021).  
 201 The specific formula is as follows.

$$202 \quad \text{SVP} = 6.112 \times (3.46 \times 10^{-6} \times P_a + 7 \times 10^{-4} + 1) \times e^{\frac{17.67 \times T_a}{T_a + 243.5}} \quad (2)$$

$$203 \quad \text{AVP} = 6.112 \times (3.46 \times 10^{-6} \times P_a + 7 \times 10^{-4} + 1) \times e^{\frac{17.67 \times T_d}{T_d + 243.5}} \quad (3)$$

$$204 \quad P_a = 1013.25 \times \left( \frac{273.16 + T_a}{273.16 + T_a + 0.0065 \times Z} \right) \times e^{5.625} \quad (4)$$

$$205 \quad \text{VPD} = \text{SVP} - \text{AVP} \quad (5)$$

206 where  $P_a$  represents atmospheric pressure estimated from elevation ( $Z$ ) and 2 m air  
 207 temperature ( $T_a$ ). Both  $T_a$  and  $T_d$  (2 m dew point temperature) were obtained from the  
 208 ERA5-Land dataset. SVP and AVP denote the saturated and actual vapor pressures  
 209 (both in kPa), respectively. Soil data included soil moisture at 0-7 cm from ERA5, as  
 210 well as soil organic carbon (SOC) and clay content at 0-10 cm from Open Land Map  
 211 (Hengl et al., 2017). Human activity indicators were represented by annual human  
 212 footprint data (Mu et al., 2022). To maintain spatial resolution consistency, we

213 performed bilinear interpolation for monthly discrete variables, nearest-neighbor  
 214 interpolation for static data and median aggregation for fire-related variables,  
 215 ultimately resampling all data to a 0.1 ° grid resolution. Detailed characteristics of  
 216 these datasets are summarized in [Table 1](#).

217 [Table 1. Data used in this study.](#)

Variable	Usage	Resolution		Period	Units	Sources
		Temporal	Spatial			
GPP	Estimation of WUE	8 days	500 m	2001-2021	$\text{g C m}^{-2}$	
ET	Estimation of WUE, Attribution analysis	8days	500 m	2001-2021	mm	<a href="#">Zhang et al., 2022</a>
Burn area	Fire intensity	Monthly	500 m	2004-2020	ha	<a href="#">Giglio et al., 2021</a>
LAI	Fire intensity	4 days	500 m	2004-2020	$\text{m}^2 \text{m}^{-2}$	<a href="#">Myneni et al., 2021</a> <a href="#">Friedl and</a>
Land cover	Zonal statistics	Yearly	0.05 °	2001-2021	\	<a href="#">Sulla-Menashe, 2022</a>
PRE	Attribution analysis	Monthly	0.5 °	2001-2021	mm	<a href="#">Harris et al., 2020</a>
TMP	Attribution analysis				°C	
Elevation	Attribution analysis	\	30 m	\	m	<a href="#">Farr et al., 2007</a>
VPD	Attribution analysis	Monthly	0.25 °	2001-2021	k Pa	<a href="#">Yao et al., 2023</a>
SOC	Attribution analysis	\	0.25 °	\	g/kg	
Clay content	Attribution analysis	\	250 m	\	% (kg / kg)	<a href="#">Hengl et al., 2017</a>
Human Footprint	Attribution analysis	Yearly	1 km	2001-2018	\	<a href="#">Mu et al., 2022</a>

218

## 219 **2.3 Methods**

### 220 **2.3.1 Ecosystem water use efficiency**

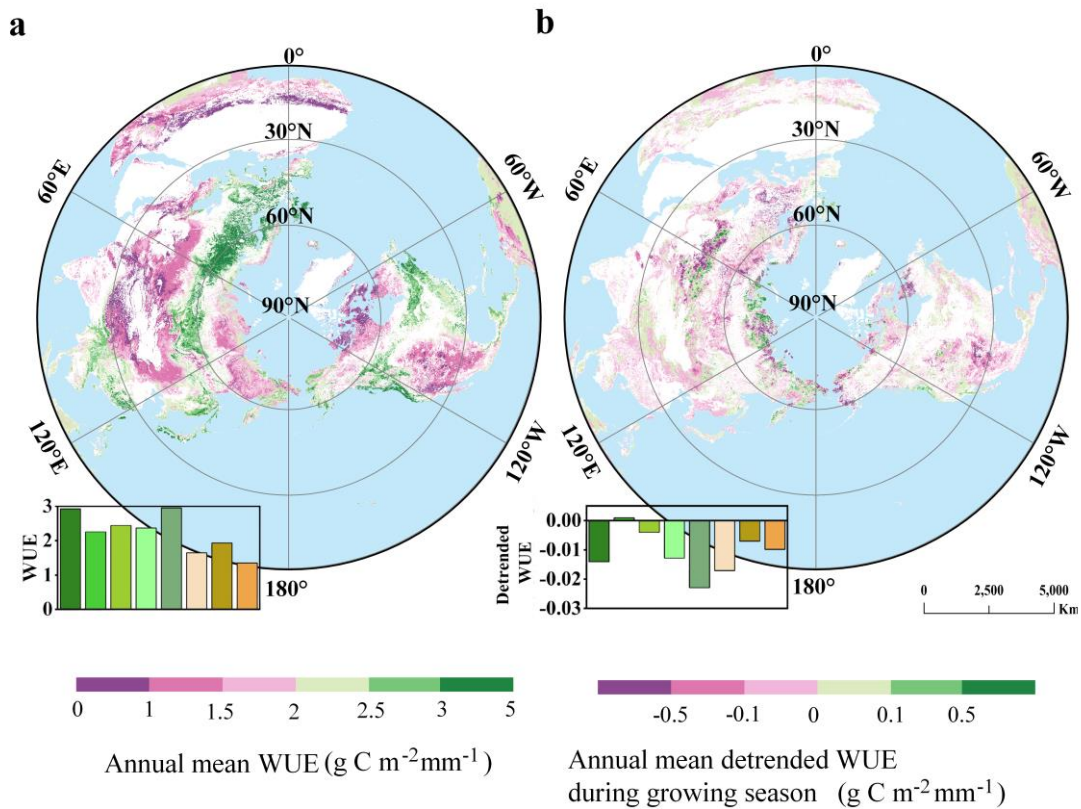
221 The WUE of an ecosystem can be defined as the ratio between the carbon

222 fixation amount (GPP) and the evapotranspiration (ET). It can be calculated as  
223 follows:

$$224 \quad \text{WUE} = \frac{\text{GPP}}{\text{ET}} \quad (6)$$

225 where WUE represents the WUE of vegetation in units of  $\text{g C m}^{-2} \text{mm}^{-1}$ , GPP denotes  
226 gross primary productivity in units of  $\text{g C m}^{-2}$ , and ET refers to transpiration in mm,  
227 respectively. After calculating the monthly WUE, we applied a detrending process  
228 because the temporal trend in WUE is driven by long-term trends, seasonality, climate  
229 forcing and autocorrelation. We applied Locally Estimated Scatterplot Smoothing  
230 (LOESS) to decompose the monthly WUE time series into trend, seasonal, and  
231 residual components. This approach aims to isolate short-term ecological responses by  
232 removing long-term trends (e.g., climate change effects) and seasonal cycles, while  
233 simultaneously addressing autocorrelation inherent in the temporal data (Abel et al.,  
234 2024). Specifically, we extracted the WUE residual component using the `stl()` function  
235 in the ‘stats’ package (v4.2.1) in the R software. In the decomposition process, we set  
236 the `s.window` parameter to ‘periodic’ to represent a fixed 12-month seasonal cycle  
237 (Wang et al., 2023), and used a trend window of 23 months (`t.window = 23`), which  
238 generated a time series of WUE residuals for each grid. For robustness, we also varied  
239 the `t.window` parameter (17 and 29 months) to evaluate the sensitivity of the residual  
240 component to the choice of different windows (Fig. S1). From a spatial perspective,  
241 the WUE patterns across these vegetation types show significant latitudinal zonal  
242 characteristics (Fig. 2a), with a clear gradient decreasing from the poles to the Equator.  
243 High-latitude coniferous forest regions generally exhibit higher WUE, as they are  
244 better adapted to cold climates and can utilize water efficiently during the limited  
245 growing season. In contrast, the average WUE in arid/semi-arid regions is lower,  
246 primarily limited by water scarcity (Tang et al., 2014; Fan et al., 2023). To evaluate  
247 the robustness of our WUE estimates to input-data selection, we additionally derived  
248 two WUE datasets, using GOSIF-GPP (Li and Xiao, 2019), FLUXCOM-GPP (Jung et  
249 al., 2020), and ERA5-Land ET (Muñoz, 2019). The spatial patterns of annual mean  
250 WUE derived from the three combinations are similar, with some deviations

251 appearing in Northern Russia and Northwestern North America (Fig. 2a, Fig. S2a, and  
 252 Fig. S3a). Apart from this localized difference, the other two WUE datasets exhibit  
 253 similar latitudinal gradients to Fig 2a (Fig. S2 and Fig. S3). After removing long-term  
 254 trends and seasonal fluctuations, the residual WUE variability reflects short-term  
 255 ecological dynamics (e.g., interannual climate anomalies or disturbance events).  
 256 Given the substantial decline in vegetation photosynthetic efficiency during the winter  
 257 months in the Northern Hemisphere, our analysis of WUE is restricted to the growing  
 258 season. The growing season was defined as the months with an average temperature  
 259 higher than 0 °C. Considering that the study area includes arid/semi-arid regions, we  
 260 further restricted the monthly precipitation of the growing season to between 10% and  
 261 90% of the annual mean total precipitation (Xu et al., 2024). We observed a declining  
 262 trend in residual WUE during growing season across most vegetation types (Fig. 2b),  
 263 and similar patterns were found in the other two WUE datasets (Fig. S2b and Fig.  
 264 S3b), suggesting potential increasing impacts of episodic disturbances (e.g., wildfires  
 265 or droughts).



266

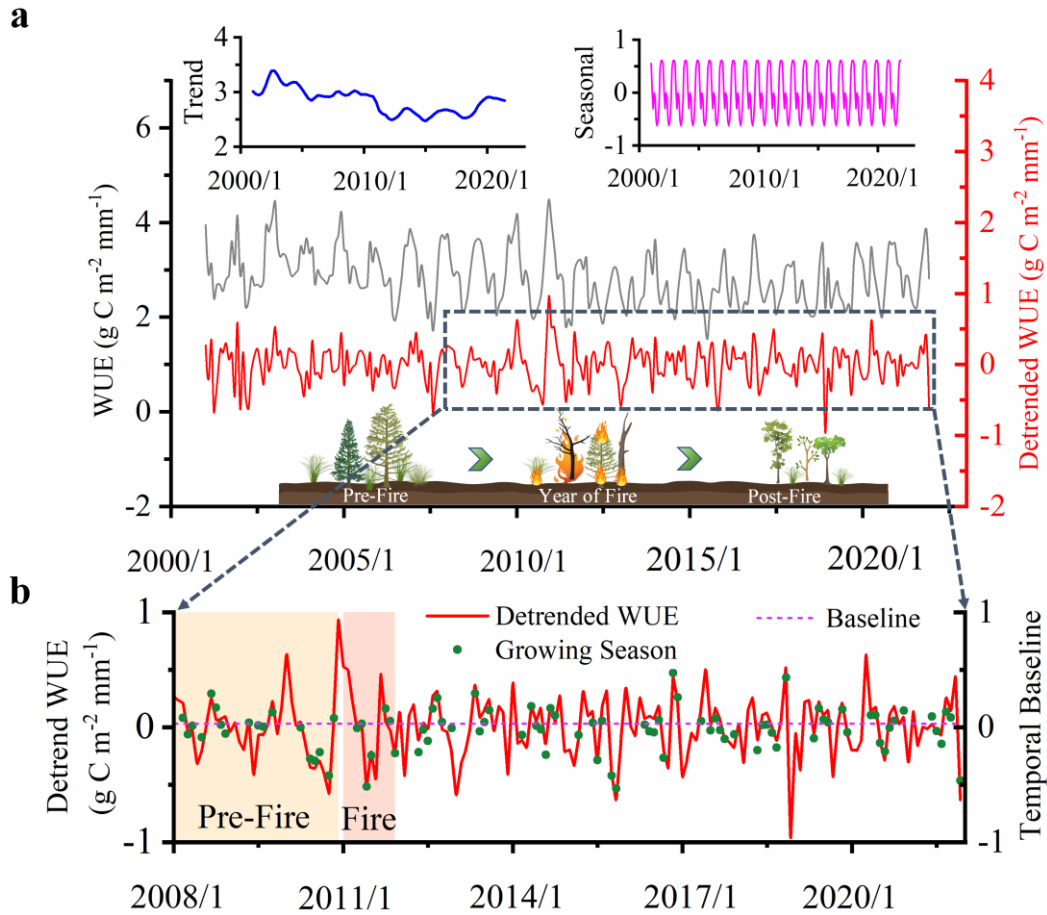
267 Fig. 2. Distribution of WUE before and after detrending. a. Annual mean spatial distribution of

268 WUE without removing long-term trends and seasonal fluctuations. b. Spatial distribution of  
269 multi-year means of WUE during the growing season after eliminating long-term trends and  
270 seasonal fluctuations. Both insets show the distribution of WUE across different vegetation types,  
271 with color schemes shared with the inset of [Fig. 1a](#).

272

### 273 **2.3.2 The temporal baseline of pre-fire WUE**

274 We analyzed the changes in WUE before and after fire at an annual scale, with a  
275 particular focus on the growing season WUE. We first extracted the WUE time series  
276 of the growing season for each burned pixel during the three years prior to the fire,  
277 removing long-term trends and seasonal fluctuations, and used the mean of this series  
278 as the preliminary time baseline. Since disturbances often lead to significant negative  
279 anomalies in WUE ([Poppe et al., 2023](#)), with fire having a more severe impact, we  
280 further excluded outliers below -0.5 standard deviations from the initial baseline to  
281 reduce the influence of disturbances such as drought or small, isolated fires ([Yao et al.,](#)  
282 [2023](#)). Finally, the remaining time series was averaged again, serving as the WUE  
283 time baseline for the burned pixel before the fire. [Fig. 3](#) presents a schematic diagram  
284 detailing the methodology for extracting the temporal baseline of WUE at a specific  
285 fire pixel, specifically focusing on WUE derived from time-series data after removing  
286 interannual trends and seasonal variations.



287  
 288 **Fig. 3.** Extraction of the pre-fire WUE temporal baseline from a given location in North America  
 289 (33.34° N, 87.05° W) where a fire disturbance occurred. a. The monthly raw WUE time series  
 290 from 2001 to 2021. The interannual and seasonal trends were first extracted from the raw WUE  
 291 using STL decomposition, and the residuals were defined as detrended WUE. b. The  
 292 corresponding time series selected to calculate WUE dynamics during the growing season before  
 293 and after a fire occurred in 2011.

294

### 295 **2.3.3 Post-fire variation in WUE**

296 To capture the changes in post-fire vegetation WUE over the longest possible  
 297 period, we based our analysis on fire pixels that experienced only one fire event  
 298 between 2004 and 2018, and constructed the time-series of WUE after the fire. The  
 299 specific formula is as follows:

$$300 \quad \Delta WUE = WUE_i - WUE_{baseline} \quad (7)$$

301 Here,  $WUE_i$  represents the WUE in the year after the fire, with time  $i$  ranging

302 from 0 to 15 years (e.g., 0 represents the year of the fire, and 15 represents the 15th  
303 year after the fire).  $WUE_{baseline}$  is the pre-fire time baseline (the specific calculation  
304 method is detailed in Section 2.3.2). Finally,  $\Delta WUE$  is the difference between the two  
305 and represents the change in WUE after the fire.

306

#### 307 **2.3.4 Attribution analysis**

308 To identify the factors controlling the post-fire WUE changes, we collected a set  
309 of environmental factors for each burned pixel over the three years following fire,  
310 using seasonal averages. These factors include temperature (TMP), precipitation  
311 (PRE), VPD, elevation, land cover type, human footprint (Footprint), soil moisture  
312 (SM), clay content, soil organic carbon (SOC), pre-fire levels of WUE and fire  
313 intensity, among others. Detailed information is provided in [Table 1](#). These factors  
314 encompass various dimensions related to WUE, including its own status, soil  
315 properties, climate conditions, and fire characteristics. Prior to analysis, seasonal  
316 fluctuations and long-term trends were removed from the monthly variables.

317 After screening, we established an XGBoost model based on the gradient  
318 boosting strategy for a total of 36,000 qualifying burned pixels from 2004 to 2018.  
319 These pixels met the following criteria: they experienced only a single fire event, their  
320 primary land cover type did not undergo changes, and the fire intensity exceeded 10%.  
321 The aim of this model was to assess the relative impact of environmental conditions  
322 on WUE changes over the five years following the fire.

323 The model was optimized through random search for hyperparameters, with the  
324 root mean squared error (RMSE) used as the evaluation criterion. The maximum tree  
325 depth was set to 10, and the learning rate was set to 0.01. Additionally, both the  
326 column sampling ratio and subsample ratio for each tree were set to 85% to enhance  
327 the model's generalization ability. We also applied L1/L2 regularization to control  
328 model complexity and used early stopping to adjust the training rounds dynamically,  
329 preventing overfitting.

330 To further quantify the relative importance of each variable, we used the built-in

331 feature importance metric of the XGBoost model. Specifically, variables were ranked  
332 based on the Gain metric, which measures the average reduction in the model loss  
333 function contributed by each variable across all decision tree splits, thereby reflecting  
334 their relative contribution to model performance. To ensure robustness, we employed  
335 the bootstrap method with 100 iterations. The variables were ranked according to their  
336 mean Gain values. This approach effectively identifies the key environmental factors  
337 that significantly contribute to WUE changes. Furthermore, we used partial  
338 dependence plots (PDP) to assess how WUE responds to each feature variable,  
339 providing clear insights into how changes in each feature influence the model's  
340 prediction outcomes. The XGBoost modeling analysis was conducted using the  
341 xgboost package (Chen and Guestrin, 2016) and the pdp package (Greenwell, 2017)  
342 in R.

343

## 344 **3. Results**

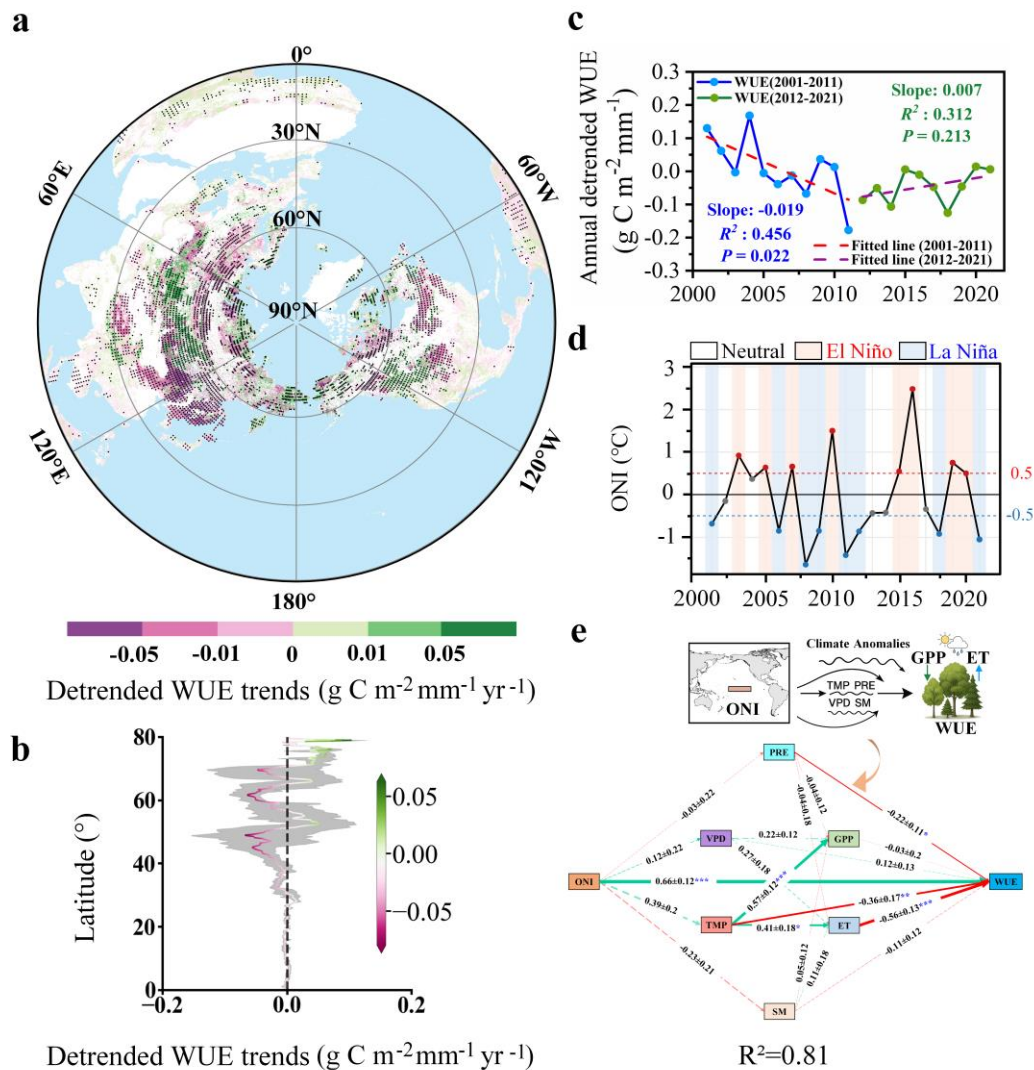
### 345 **3.1 Spatiotemporal evolution in detrended WUE**

346 We systematically assessed the spatiotemporal evolution of WUE during the  
347 growing season over the past two decades, focusing on eight land cover types that  
348 remained stable without significant land use changes. This approach effectively  
349 minimizes the potential confounding effects of land use change on the observed WUE  
350 dynamics. The analysis of the annual mean WUE values after de-trending revealed a  
351 significant inflection point in 2011 (Fig. 4c). Specifically, from 2001 to 2011, WUE  
352 exhibited a notable downward trend ( $-0.019 \text{ g C m}^{-2} \text{ mm}^{-1} \text{ yr}^{-1}$ ), while since 2011,  
353 WUE has shown a non-significant increase ( $0.007 \text{ g C m}^{-2} \text{ mm}^{-1} \text{ yr}^{-1}$ ). The statistical  
354 insignificance of this post-2011 trend was not affected by the choice of LOESS  
355 decomposition parameters (Fig. S3 and Fig. S4). A similar turning point is also  
356 observed across multiple ecosystem types, including evergreen needleleaf forests  
357 (ENF), deciduous broadleaf forests (DBF), mixed forests (MF), and savannas (SAV)  
358 (Fig. S6). By integrating annual atmospheric circulation anomalies with climate

359 anomaly datasets, specifically the interannual anomalies of detrended growing-season  
360 variables (TMP, PRE, VPD, SM, GPP, and ET) (Fig. S7), we developed a simplified  
361 path-analysis model to identify the teleconnection pathways. This model reveals how  
362 large-scale circulation anomalies and climate disturbances shape interannual  
363 variations in WUE (Fig. 4e, Fig. S4e, and Fig. S5e). The results show that large-scale  
364 circulation indicators, including the Oceanic Niño Index (ONI) (He et al., 2025) and  
365 the 850 hPa zonal wind (u850) (Qiu et al., 2025), are significantly positively  
366 correlated with WUE, with standardized coefficients of 0.66 and 0.65, respectively  
367 (Fig. 4e and Fig. S8). Moreover, because wintertime ONI values indicate ENSO  
368 phases, we identified the types of extreme ENSO events occurring between 2001 and  
369 2021 based on National Oceanic and Atmospheric Administration (NOAA)  
370 classification standards (Fig. 4d) (NOAA National Weather Service, Climate  
371 Prediction Center, 2024). Both the path analysis and the temporal sequence of ENSO  
372 extremes suggest that the 2011 inflection point may have been influenced by the La  
373 Niña event occurred around 2011 (Fig. 4d, Fig. S4d, and Fig. S5d). In addition, we  
374 found significant negative correlations between ET, PRE, and WUE (Fig. 4e, Fig. S4  
375 e, and Fig. S5e), indicating that climate anomalies induced by extreme events exert  
376 substantial influence on vegetation water-use strategies. Such extreme circulation  
377 anomalies could reorganize climate patterns across the Northern Hemisphere  
378 (Boening et al., 2012; Blunden and Arndt, 2012), potentially amplifying the divergent  
379 vegetation responses between humid and arid regions and, consequently, modifying  
380 water-use efficiency (Bonfils et al., 2017; Jin et al., 2025).

381 Moreover, non-parametric tests, including the Mann-Kendall (MK) test (Yue et  
382 al., 2002) and Theil-Sen trend analysis (Sen, 1968), were applied to spatially assess  
383 the overall trend in vegetation WUE. In regions where the trend was statistically  
384 significant ( $P < 0.05$ ), WUE exhibited a notable decreasing trend of  $-0.016 \text{ g C m}^{-2}$   
385  $\text{mm}^{-1} \text{ yr}^{-1}$ . However, substantial differences were observed among different forests  
386 types (Fig. 4a). Specifically, a significant decrease in WUE was observed in  
387 coniferous forests in the Russian Far East and Northern Europe, whereas a significant  
388 increase was found in broadleaf forests in Siberia and coniferous forests near the

389 Rocky Mountains in North America. From a latitudinal perspective, trends in  
 390 detrended WUE below 30° latitude were mostly not significant, with two main  
 391 regions of decline observed between 40° and 50° latitude, and again between 60° and  
 392 70° latitude, followed by an overall increase above 70° latitude (Fig. 4b). These  
 393 results suggest that both vegetation type and geographic location play critical roles in  
 394 shaping the spatial patterns of WUE, potentially linked to recent vegetation greening  
 395 and permafrost thawing in near-polar regions.



396  
 397 **Fig. 4.** Interannual trends and spatial distribution of detrended WUE in the study area. a. The  
 398 change slopes of WUE from 2001 to 2021 across the Northern Hemisphere, with black markers  
 399 indicating significance at the 95% confidence level. b. Interannual fluctuations of WUE. c. The  
 400 latitude profile of the WUE slope from panel a, with shaded areas representing the 95%  
 401 confidence interval of the WUE trend. d. Annual winter ONI index and associated extreme ENSO

402 events, with dashed horizontal lines indicating the ONI thresholds ( $\pm 0.5$  °C) used to identify El  
403 Niño and La Niña events. e. Schematic of the path-analysis model illustrating how ONI anomalies  
404 in the central-eastern equatorial Pacific (Niño 3.4) influence terrestrial WUE. Red paths denote  
405 negative effects, whereas green paths indicate positive effects. Each path is labeled with its  
406 standardized coefficient and significance level.

407

### 408 **3.2 Change of post-fire WUE**

409 To assess the impact of fire on WUE, we calculated the five-year post-fire  
410 average  $\Delta$ WUE for all burned pixels between 2004 and 2020, and mapped the results  
411 at a  $0.5^\circ$  spatial resolution (Fig. 5a). The mean  $\Delta$ WUE across all fire-affected pixels  
412 was  $0.0025 \text{ g C m}^{-2} \text{ mm}^{-1}$ . Although the overall average change appears limited in  
413 magnitude, the distribution of pixel-level responses reveals a clear pattern: the  
414 proportion of pixels with negative  $\Delta$ WUE responses following fire, relative to pre-fire  
415 WUE levels, was higher than that of pixels with positive responses (Fig. 5b).  
416 Approximately 74.2% of pixels exhibited  $\Delta$ WUE values ranging from  $-0.5$  to  $0.5 \text{ g C}$   
417  $\text{m}^{-2} \text{ mm}^{-1}$ , with a noticeable bias toward negative values. We further evaluated  
418 fire-induced changes using two additional WUE datasets, including the  
419 GOSIF-ERA5-based WUE and FLUXCOM-ERA5-based WUE. It is found that 75.8%  
420 of pixels in the GOSIF-ERA5-based WUE and 85.1% in the  
421 FLUXCOM-ERA5-based WUE also fell within this range, again with a higher  
422 proportion of negative values (Fig. S9b and Fig. S10b). These results consistently  
423 indicate that fire disturbances tended to result in adverse WUE responses across large  
424 areas.

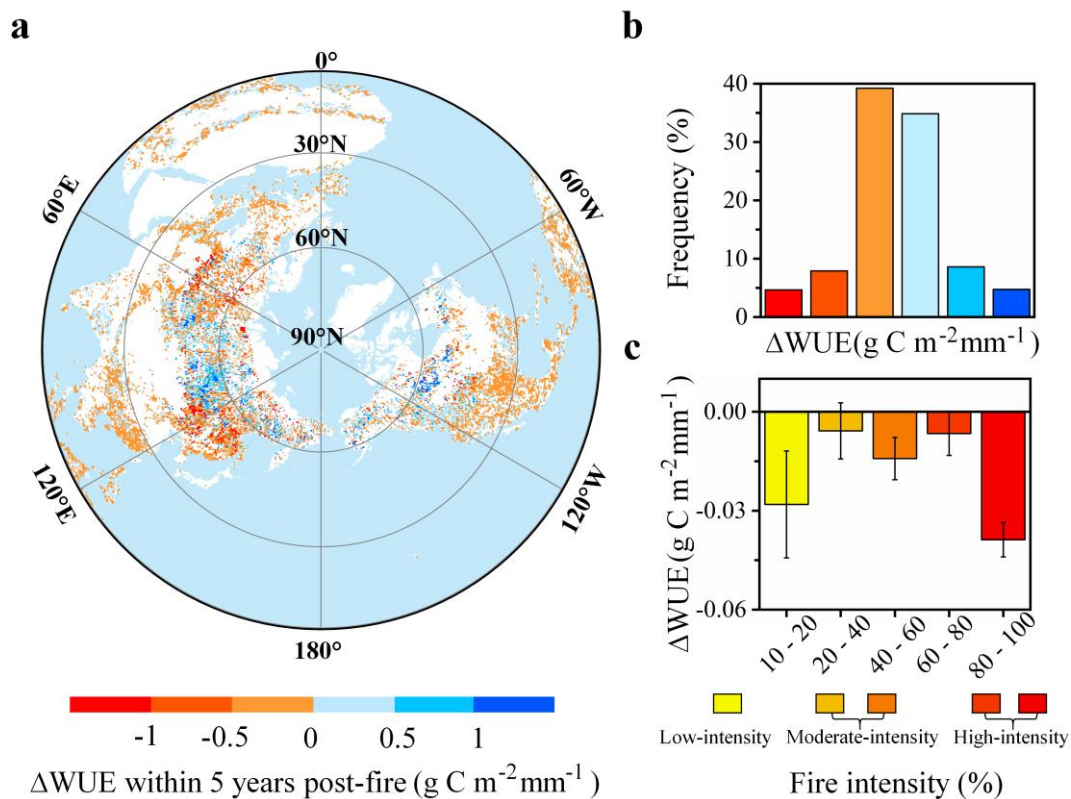
425 Spatial patterns showed that post-fire reductions in WUE were widespread, with  
426 particularly strong signals in high-latitude regions (Fig. 5a). Notably, the Russian Far  
427 East exhibited extensive areas with negative  $\Delta$ WUE values, indicating sustained  
428 declines following fire. These areas are predominantly located within transition zones  
429 between coniferous and mixed forests (Fig. 1a). Similar trends were observed across  
430 northeastern China and the Korean Peninsula, where negative  $\Delta$ WUE responses were

431 spatially coherent. In central Canada and northern parts of the United States, extensive  
432 regions also showed declines in WUE, particularly within forest-grassland ecotones.  
433 These patterns are consistent with previous findings indicating that post-fire recovery  
434 in boreal and temperate ecosystems is often constrained by climatic and edaphic  
435 conditions, including prolonged soil freezing and reduced water availability (Liu et al.,  
436 2024).

437 In contrast, positive  $\Delta$ WUE values were mainly clustered in eastern Siberia and  
438 northern North America. These areas were largely dominated by coniferous forests,  
439 with deciduous conifer types in eastern Siberia showing comparatively stronger  
440 positive  $\Delta$ WUE responses, while evergreen conifers in northern North America  
441 exhibited more moderate positive responses. The contrasting responses across  
442 vegetation types suggest that fire-induced changes in WUE likely reflect differences  
443 in vegetation recovery and water use strategies.

444 We further evaluated the relationship between fire intensity and WUE response  
445 (Fig. 5c), and found that  $\Delta$ WUE remained negative across all intensity levels. For  
446 instance, low-intensity fires (10–20%) resulted in an average  $\Delta$ WUE of approximately  
447  $-0.025 \text{ g C m}^{-2} \text{ mm}^{-1}$ , while the most intense fires (80–100%) were associated with  
448 the largest reductions, reaching  $-0.04 \text{ g C m}^{-2} \text{ mm}^{-1}$ . Intermediate fire intensities (20–  
449 80%) produced relatively smaller changes. This nonlinear relationship between fire  
450 intensity and  $\Delta$ WUE may be explained by threshold responses and compensatory  
451 mechanisms in ecosystem carbon–water dynamics. At low intensity, partial canopy  
452 scorch and litter consumption depress photosynthetic capacity without proportionally  
453 reducing evapotranspiration, because exposed soil enhances direct evaporation and  
454 reduces rainfall interception, resulting in a small but consistent decline in WUE  
455 (Valor et al., 2018; Shakesby and Doerr, 2006). At intermediate severities, surviving  
456 vegetation and rapid resprouting maintain proportional reductions in carbon  
457 assimilation and water use, and resource release such as light, nutrients, and soil  
458 moisture may stimulate compensatory growth, thereby buffering the decline in WUE  
459 (Clarke et al., 2013; Tangney et al., 2022). By contrast, high-intensity fires cause  
460 near-complete vegetation loss, leading to a collapse of carbon uptake while

461 evaporation from exposed soils persists, often exacerbated by soil hydrophobicity and  
 462 delayed regeneration, resulting in the strongest WUE reduction (Hubbert et al., 2012;  
 463 Bär et al., 2019; Madani et al., 2021; Fernández-Guisuraga et al., 2025). This  
 464 nonlinear response suggests that ecosystems maybe more vulnerable at low and high  
 465 fire severities, where canopy damage or stand-replacing fire disrupts carbon–water  
 466 coupling, while moderate burns allow partial resilience and more efficient resource  
 467 use.



468  $\Delta WUE$  within 5 years post-fire ( $\text{g C m}^{-2} \text{mm}^{-1}$ )  
 469 **Fig. 5.**  $\Delta WUE$  and its relationship with fire intensity within 5 years after the fire. a. Spatial  
 470 distribution of  $\Delta WUE$ , for display, we aggregated the results from 2004 to 2018 to a resolution of  
 471  $0.5^\circ$ . b. Frequency distribution of each  $\Delta WUE$  interval. c. Distribution characteristics of  $\Delta WUE$   
 472 under different fire intensities.

473

### 474 **3.3 The trajectories of WUE by vegetation type**

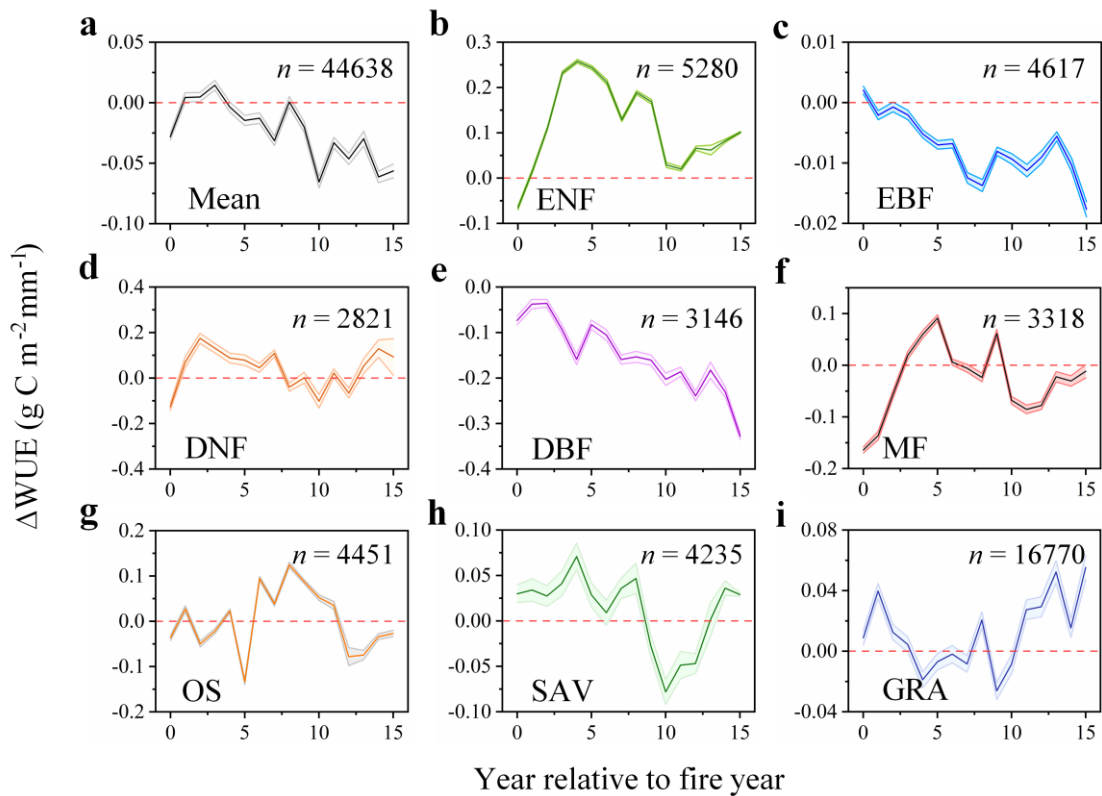
475 We analyzed post-fire  $\Delta WUE$  trends over a 15-year period across dominant  
 476 vegetation classes. The results show that WUE fluctuates markedly during the first

477 five years following fire. Specifically, in the fire year (Year 0),  $\Delta$ WUE is already  
478 negative, which may reflect the compound effects of fire and concurrent drought  
479 stress. Combined with the changes in GPP and ET during the same period, it can be  
480 found that both are lower than the pre-fire levels (Fig. S11a and Fig. S12a). In the  
481 subsequent three years, WUE increases rapidly, temporarily exceeding pre-fire levels  
482 by the third year, likely due to the enhanced photosynthetic capacity and fast recovery  
483 of GPP during the seedling establishment phase. However, starting from the fourth  
484 year, WUE declines sharply, which may be associated with increasing ecosystem  
485 evapotranspiration as vegetation structure becomes denser. In terms of long-term  
486 trends, compared to pre-fire conditions, WUE shows a sustained decline beginning  
487 around the fourth-year post-fire (Fig. 6), reaching its lowest point in the tenth year  
488 ( $-0.06 \text{ g C m}^{-2} \text{ mm}^{-1}$ ). These interannual fluctuations indicate that the changes in  
489 WUE after fire disturbance are dramatic and that recovery can be prolonged or vary  
490 greatly depending on the region and environmental conditions.

491 The differentiated responses of various vegetation types to changes in WUE  
492 following fire disturbance were also revealed. The results show that, overall,  
493 coniferous forests, particularly evergreen coniferous forests (ENF), reach post-fire  
494 WUE levels above the pre-fire baseline early after fire, and maintain elevated levels  
495 throughout the 15 years following fire. This phenomenon may be closely related to  
496 their biophysical characteristics and regeneration strategies. Coniferous forests, due to  
497 their high resin content, are highly flammable (Rogers et al., 2015), making them  
498 vulnerable to high-intensity fire events, which often kill or damage the vegetation and  
499 result in a sharp reduction in transpiration (Nolan et al., 2014). However, during the  
500 post-fire regeneration phase, young seedlings may exhibit higher WUE. Furthermore,  
501 other environmental factors may influence the trajectory of WUE after fire. For  
502 example, coniferous forests may enhance WUE by optimizing respiration and light  
503 conditions during the growing season (Tang et al., 2017; Dukat et al., 2024).  
504 Nevertheless, this trend is not uniform and is strongly modulated by climate (Fig.  
505 S13). When stratified by the Köppen-Geiger climatic zones (Beck et al., 2018), the  
506 strongest positive  $\Delta$ WUE responses are observed in cold-region ENF (Fig. S13c). In

507 contrast, temperate ENF shows weaker post-fire positive  $\Delta$ WUE responses and  
508 exhibits negative  $\Delta$ WUE responses (Fig. S13d).

509 The differences in WUE trajectories caused by climate zone differences are also  
510 evident in broadleaf forest types. Overall, broadleaf forests generally show negative  
511  $\Delta$ WUE responses following fire (Fig. 6c, e). By analyzing the synchronous dynamics  
512 of ET and GPP, it is seen that transpiration can usually recover rapidly to pre-fire  
513 levels, which may be related to the high stomatal conductance and transpiration rate  
514 of broad-leaved tree species (Li et al., 2025). In contrast, the recovery of  
515 photosynthetic capacity is slower. Specifically, GPP in deciduous broadleaf forests  
516 (DBF) returns to pre-fire levels approximately eight years after burning (Fig. S11e).  
517 In evergreen broadleaf forests (EBF), however, GPP remains persistently lower than  
518 pre-fire levels, while transpiration stays relatively high (Fig. S11c and Fig. S12c).  
519 This imbalance likely contributes to sustained negative  $\Delta$ WUE responses, despite the  
520 possibility of WUE temporarily exceeding pre-fire levels during the early post-fire  
521 stage (Fig. 6e). Upon further stratification by climate zone, it is found that the WUE  
522 trajectory of cold-region DBF dominates the overall pattern for this forest type,  
523 thereby obscuring the post-fire fluctuations observed in temperate DBF (Fig. S13f). In  
524 contrast, the WUE trajectories of temperate and tropical EBF show no significant  
525 differences (Fig. S13g, h). This difference highlights the contrasting adaptive  
526 mechanisms of coniferous and broadleaf forests in response to fire disturbance.  
527 Interestingly, for low-stature herbaceous vegetation types (such as shrubs, sparse  
528 woodlands, and grasslands), the WUE changes exhibit greater complexity. Due to  
529 their short growth cycles, the WUE of these vegetation types typically fluctuates  
530 around pre-fire levels following fire disturbances. This also suggests that their WUE  
531 is more susceptible to other disturbances, such as drought (Ahmad et al., 2024).



532

533 **Fig. 6.** Evolutionary trajectory of  $\Delta WUE$  over 1 to 15 years post-fire for different vegetation types,  
 534 with shaded areas representing the 95% confidence interval for each section. The first one shows  
 535 the average of  $\Delta WUE$ , and the rest shows the  $\Delta WUE$  in each vegetation type. The abbreviations of  
 536 vegetation types are consistent with [Fig. 1a](#).

537

## 538 **4. Discussion**

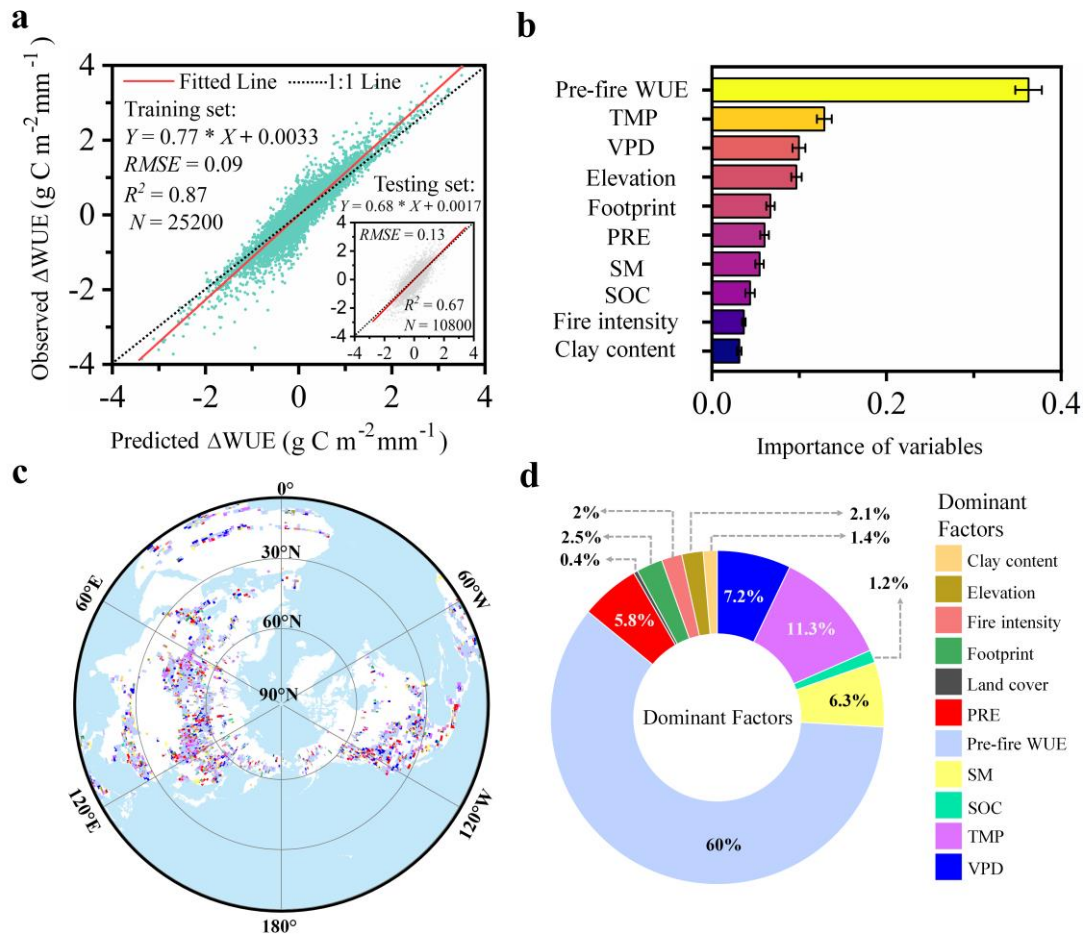
### 539 **4.1 Environmental factors influencing WUE**

540 To understand the environmental factors influencing changes in WUE after fire,  
 541 we trained an XGBoost model based on over 70% of the burned pixels from 2004 to  
 542 2018 to predict  $\Delta WUE$  post-fire ([Fig. 7](#)). The results revealed an  $R^2$  value of 0.87 on  
 543 the training set and 0.67 on the test set, indicating that the selected indicators explain a  
 544 significant proportion of the variance in  $\Delta WUE$  ([Fig. 7a](#)). Through relative  
 545 importance analysis, we ranked and evaluated the top 10 environmental factors. The  
 546 results suggest that the pre-fire WUE level is one of the key indicators influencing  
 547 post-fire WUE changes, which is expected, as the pre-fire vegetation health status

548 reflects directly its baseline WUE (Fig. 7b). Although  $\Delta$ WUE is mathematically  
549 related to pre-fire WUE, a supplementary analysis excluding this factor showed that  
550 the contributions of other environmental drivers changed little (Fig. S14), indicating  
551 that its inclusion does not obscure their roles but rather provides important ecological  
552 context. From an ecological perspective, pre-fire WUE serves as an integrative  
553 indicator of vegetation functional status, capturing multiple dimensions of ecosystem  
554 status such as carbon-water coupling efficiency, water-use capacities, and  
555 physiological stress levels (Ito and Inatomi, 2012; Yang et al., 2020). High pre-fire  
556 WUE typically indicates efficient stomatal regulation, strong photosynthetic capacity,  
557 and favorable water status that can facilitate faster vegetation recovery after burning.  
558 However, in some drought-prone grassland ecosystems, high WUE may instead  
559 reflect water-saving strategies induced by drought stress rather than a healthy  
560 ecological state (Ganjurjav et al., 2022; Zhao et al., 2020). Overall, pre-fire WUE  
561 reflects the physiological and functional condition of vegetation and, together with  
562 post-fire environmental changes, governs the direction and magnitude of shifts in  
563 WUE following fire. Therefore, we regard it as an indicator of pre-fire vegetation  
564 state with ecological significance and early warning potential (Zhang et al., 2024).  
565 Additionally, climate variables such as TMP and VPD were identified as significant  
566 influencing factors.

567 To further investigate the spatial heterogeneity of environmental controls on  
568  $\Delta$ WUE, we applied a local XGBoost modeling approach using a  $5 \times 5$  pixel moving  
569 window. This window size (about  $50 \text{ km}^2$ ) has been widely used in previous fire  
570 studies to approximate the spatial extent of relatively homogeneous climate conditions  
571 (Liu et al., 2019; Zhao et al., 2024), and our sensitivity tests with alternative sizes  
572 ( $4 \times 4$  and  $6 \times 6$ ) showed little effect on the results (Fig. S15). This method identified the  
573 dominant factor influencing WUE change at each pixel based on surrounding  
574 conditions, allowing us to capture fine-scale, context-dependent variability. The  
575 spatial distribution of dominant factors (Fig. 7c) reveals that pre-fire WUE level was  
576 the leading driver across approximately 60% of the burned areas in the Northern  
577 Hemisphere. Other influential variables included temperature (TMP, 11.3%), vapor

578 pressure deficit (VPD, 7.2%), soil moisture (SM, 6.3%), and precipitation (PRE,  
579 5.8%), while remaining factors each accounted for less than 3% of the area (Fig. 7d).  
580 These results suggest that while pre-disturbance vegetation condition plays a major  
581 role in shaping post-fire WUE trajectories, post-fire climate factors such as  
582 atmospheric dryness and water availability also contribute significantly at local scales.  
583 However, due to limited data availability in certain regions—particularly the Russian  
584 Far East and the Korean Peninsula—some spatially discrete fire-affected pixels were  
585 not well represented in the final model outputs. This limitation mainly reflects the  
586 patchy distribution of fires. Coupled with the identified filtering criteria, a number of  
587 small-sized burned areas may be ignored (Fig. S16a). While missing fire events can  
588 increase local uncertainty, our thresholding and aggregation strategies ensured that, to  
589 some extent, the retained windows remained representative of local conditions. The  
590 overall model performance ( $R^2 = 0.6-0.9$  across most regions) and the consistency of  
591 spatial patterns support the main conclusions (Fig. S16b). Given the 11 independent  
592 variables in the model, we established a minimum data-availability threshold of 40%  
593 within each  $5 \times 5$  window, corresponding to at least 10 valid pixels, to maintain  
594 regression stability. We further evaluated model performance across a range of  
595 thresholds and found that the 40% criterion effectively captures local variability while  
596 preventing substantial degradation in model accuracy or too few effective pixels (Fig.  
597 S17 and Fig. S18). These findings offer valuable insights into the mechanisms  
598 regulating post-fire WUE dynamics and highlight the importance of both antecedent  
599 vegetation condition and local climate constraints during ecosystem recovery.



600

601 **Fig. 7.** Model interpretability and the relative importance of variables based on the XGBoost  
 602 model. a. The model's performance on the training (main plot) and testing (inset) datasets (the unit  
 603 of RMSE is  $\text{g C m}^{-2} \text{mm}^{-1}$ ). b. The top 10 most influential environmental factors ranked by  
 604 importance, quantified using the XGBoost built-in Gain metric. c. Spatial distribution of the  
 605 dominant environmental drivers of post-fire  $\Delta WUE$  based on local XGBoost modeling across the  
 606 Northern Hemisphere. d. Area proportions of dominant factors.

607

## 608 4.2 Response of WUE to environmental variables

609 The response functions from the trained global XGBoost model, shown as partial  
 610 dependence plots, describe the marginal effects of environmental variables on  $\Delta WUE$ .  
 611 These plots help to analyze the specific mechanisms through which these  
 612 environmental factors influence  $\Delta WUE$  after a fire (Fig. 8). First, the pre-fire WUE  
 613 status exerts a strong influence on vegetation recovery trajectories. Low pre-fire WUE

614 may indicate that vegetation already experienced physiological stress such as  
615 drought-induced stomatal closure or reduced carbon assimilation prior to burning (Li  
616 [et al., 2025](#)). Under such conditions, post-fire dynamics are often characterized by  
617 compensatory positive  $\Delta$ WUE responses, as vegetation re-establishes photosynthetic  
618 capacity and carbon-water balance. In contrast, high pre-fire WUE generally reflects  
619 vegetation with efficient water use and strong photosynthetic activity. Such conditions  
620 may also correspond to greater fuel loads, as observed in Alaskan Arctic tundra  
621 ecosystems where higher pre-fire greenness is associated with increased fire intensity  
622 ([Chen et al., 2024](#)). Consequently, after fire, these areas may exhibit larger declines in  
623 WUE because the damage to well-developed canopies and hydraulic structures is  
624 more substantial, leading to slower recovery and reduced carbon–water coupling  
625 efficiency.

626 Additionally, the response curve for temperature (TMP) reveals a significant  
627 threshold effect in temperature changes on post-fire WUE dynamics. Both large  
628 increases and decreases in temperature hinder the maintenance of favorable WUE  
629 states after a fire. This is consistent with previous studies, which suggests that  
630 moderate temperature ranges are conducive to maintaining a stable vegetation growth  
631 state ([Cunningham and Read, 2003](#)). However, rapid temperature changes, such as  
632 heatwaves, can significantly alter the photosynthetic rate and water use strategies of  
633 vegetation ([Teskey et al., 2015](#)). Previous research has indicated that the VPD  
634 significantly regulates vegetation water use and photosynthetic rates ([Yuan et al.,](#)  
635 [2019](#)). Our research confirms that lower VPD (i.e., higher humidity) is associated  
636 with relatively higher post-fire WUE. As VPD increases, negative  $\Delta$ WUE responses  
637 become more pronounced, indicating that drier conditions may weaken post-fire WUE.  
638 This may be due to higher evaporative demand and suppressed photosynthesis under  
639 elevated atmospheric dryness. Additionally, the effect of altitude on post-fire  $\Delta$ WUE  
640 also shows a clear threshold range. Both low and high altitudes are associated with  
641 negative  $\Delta$ WUE responses.

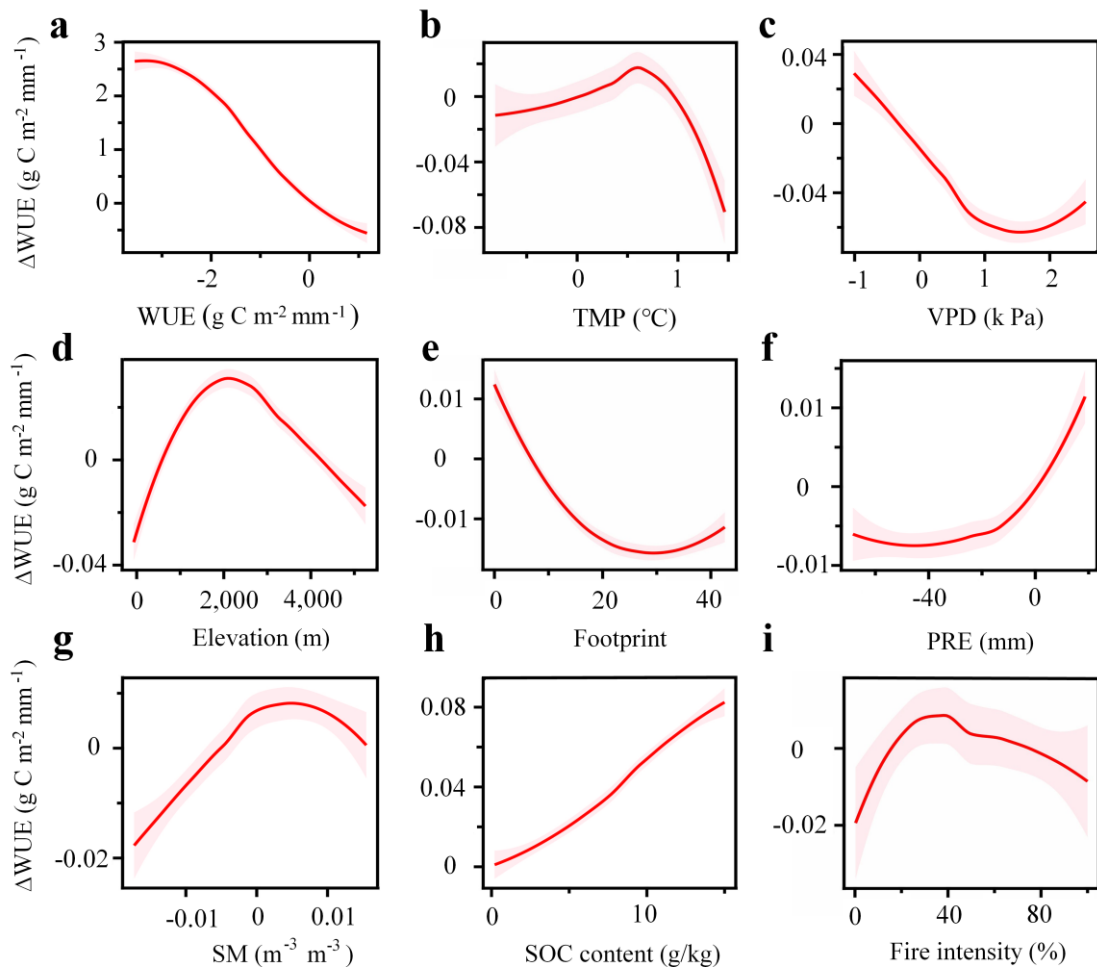
642 We made efforts from the outset to exclude regions with significant human  
643 activity. To minimize the influence of human activity, our analysis was restricted to

644 pixels dominated by natural vegetation cover that had not undergone land cover  
645 change during the study period. Urban, agricultural, and other human-modified areas  
646 were excluded based on land cover classifications. However, to account for potential  
647 residual human influence within the remaining natural areas, we incorporated a  
648 human footprint index into the modeling framework. The results show that higher  
649 human footprint values are associated with negative  $\Delta$ WUE responses in post-fire  
650 vegetation recovery. Human activity, such as irrigation, fertilization, afforestation,  
651 thinning and prescribed fires, can influence WUE in both positive and negative ways  
652 (Martin et al., 2010; Paris et al., 2018). However, in areas with low human activity,  
653 natural vegetation recovery may be more conducive to improving post-fire WUE.

654 The effects of precipitation and soil moisture changes on  $\Delta$ WUE exhibit similar  
655 patterns. In regions with reduced precipitation,  $\Delta$ WUE shows predominantly negative  
656 responses and remains at relatively low post-fire levels. However, as precipitation  
657 increases,  $\Delta$ WUE shifts from negative to positive values, indicating that post-fire  
658 WUE exceeds pre-fire levels. A similar pattern is observed for soil moisture: arid  
659 environments are associated with negative  $\Delta$ WUE responses. Previous studies have  
660 confirmed that dry environments can significantly weaken vegetation stomatal  
661 behavior and carbon assimilation processes (McDowell, 2011), leading to a decrease  
662 in WUE. However, the geographical impact of drought stress is complex. For example,  
663 in some arid regions, WUE increases with the degree of drought, while in semi-arid  
664 and humid regions, drought stress leads to a decline in WUE (Yang et al., 2016).

665 Analysis of the response curve based on SOC suggests that post-fire vegetation  
666  $\Delta$ WUE tends to increase with SOC content. This indicates that soil carbon reserves  
667 are associated with higher post-fire WUE levels, possibly by improving soil structure  
668 and enhancing nutrient supply, thus, promoting vegetation growth and recovery. The  
669 impact of fire intensity is consistent with previous findings (see Section 3.2), with  
670 both low and high intensity fires exerting negative effects on post-fire WUE.

671 In summary, the mechanisms behind the effects of environmental variables on  
672 post-fire WUE changes are complex, involving both positive and negative influences,  
673 with certain threshold effects, as quantified here.



675

676 **Fig. 8.** Relationship between post-fire  $\Delta$ WUE and environmental factors. These factors are ranked  
 677 by relative importance and include pre-fire WUE, TMP, VPD, elevation, Footprint, PRE, SM,  
 678 SOC, and fire intensity. The lines represent the average response function of the XGBoost model  
 679 for each variable. The shaded areas indicate the 95% confidence interval of  $\Delta$ WUE.

680

### 681 **4.3 Limitations**

682 There remain certain uncertainties in understanding the WUE response of  
 683 northern vegetation to fire disturbances:

684 **1. Tree species differences:** Although our analysis is based on eight major  
 685 vegetation types, important physiological differences among species within each type  
 686 may still be overlooked. Trees generally exhibit higher WUE than herbaceous or  
 687 shrub vegetation (Xiao et al., 2013), yet substantial variation exists among forest types.

688 Plantation forests often show lower WUE than natural forests (Sun et al., 2024), while  
689 evergreen forests typically display higher WUE than deciduous forests (Tang et al.,  
690 2014). However, these relationships are not universal; even the same species can  
691 exhibit pronounced regional differences in WUE under contrasting climatic and  
692 hydrological conditions (Zhang et al., 2023; Medlyn et al., 2017) (Fig. S13). Fire can  
693 alter the distribution of tree species and seedlings, thereby shifting local dominance  
694 (Hill and Field, 2021), and such species turnover can further complicate the WUE  
695 patterns. In addition, remote sensing evidence suggests that woody plant expansion  
696 may locally enhance ecosystem-scale WUE (Deng et al., 2022). Therefore, species  
697 composition and successional dynamics may influence the interpretation of WUE  
698 dynamics.

699 **2. Forest age:** Forest age also influences water-use strategies. High-severity fires  
700 reset stand age, leading to shifts in WUE. Previous studies showed that WUE in  
701 evergreen forests generally peaks at mature stages (approximately 80-100 years),  
702 whereas deciduous forests exhibit a continuous increase in WUE with age (Xu et al.,  
703 2020). However, these age-related patterns are not universal. In some cases, seedlings  
704 of pine species with inherently conservative water-use strategies may exhibit higher  
705 WUE than mature individuals (Skubel et al., 2015).

706 **3. Coarse spatial resolution:** Fire intensity and WUE were aggregated to a 0.1 °  
707 spatial resolution to explore WUE trajectories after fire disturbances. However, this  
708 coarser resolution may also capture other disturbances (e.g., drought or extreme  
709 precipitation), which were not considered in this research.

710 **4. Study time frame limitations:** The study period of 2004–2020 may not be  
711 long enough to observe full vegetation recovery. Previous research indicates that  
712 while primary productivity may recover within a few years (Xu et al., 2024), biomass  
713 recovery in northern vegetation can take several decades (Wang et al., 2021). Thus,  
714 the WUE trajectory in this research is likely limited to the early stages of vegetation  
715 community recovery.

716 **5. Impact of land use changes:** While land use undoubtedly influences the  
717 post-fire WUE trajectory, this research did not account for this factor. Fires are a

718 driving force for changes in land cover (Wu et al., 2023), and large fires may lead to  
719 shifts in dominant species. Therefore, future studies should consider the impact of  
720 fire-driven vegetation type changes on post-fire WUE trajectories.

721

## 722 **5. Conclusion**

723 This research analyzed systematically the spatial distribution of temporal trends  
724 in WUE and its response to fire disturbances for Northern Hemisphere vegetation  
725 during the growing season, based on WUE data from 2001 to 2021 and fire data from  
726 2004 to 2018. By removing long-term trends and seasonal fluctuations, we were able  
727 to examine the trajectory of WUE after fire disturbances. The results reveal that, from  
728 2001 to 2021, the WUE of Northern Hemisphere vegetation generally showed a  
729 pattern of significant initial decline followed by a marked increase, with an annual  
730 average change rate of  $-0.016 \text{ g C m}^{-2} \text{ mm}^{-1} \text{ yr}^{-1}$ . However, under fire disturbances,  
731 most vegetation exhibited short-term fluctuations in WUE within the first five years.  
732 Notably, there were significant differences in the response of various vegetation types  
733 to fire disturbances: coniferous forests exhibited a sustained increase in WUE  
734 post-fire, while broadleaf forests showed a decreasing trend, and herbaceous  
735 vegetation displayed fluctuating changes. These trajectories reflect differences in  
736 water use strategies across vegetation types.

737 Further analysis revealed that environmental factors significantly influenced the  
738 WUE trajectories. Attribution analysis identified pre-fire levels of WUE as a key  
739 factor in regulating post-fire trajectories, while drought-heat stress factors, such as  
740 temperature and VPD, also played a significant role in WUE dynamics. Given that the  
741 recovery period for Northern Hemisphere vegetation, particularly forests, can span  
742 several decades before full recovery is achieved, management strategies for  
743 afforestation and assisted vegetation recovery should ensure the balance between  
744 carbon assimilation and water use. This dual consideration is especially crucial in the  
745 early stages of recovery following a fire, where optimizing both carbon uptake

746 capacity and water-use strategies will be beneficial for enhancing long-term  
747 vegetation resilience and ecosystem functions.

## 748 **Disclosure statement**

749 No potential conflict of interest was reported by the author(s).

## 750 **Funding**

751 This research was supported by the National Natural Science Foundation of China  
752 under Grants 42222108 and 42171345.

## 753 **References**

- 754 Abel, C., Maestre, F.T., Berdugo, M., Tagesson, T., Abdi, A.M., Horion, S., Fensholt, R., 2024.  
755 Vegetation resistance to increasing aridity when crossing thresholds depends on local  
756 environmental conditions in global drylands. *Commun. Earth Environ.* 5, 379.  
757 <https://doi.org/10.1038/s43247-024-01546-w>.
- 758 Ahmad, S.K., Holmes, T.R., Kumar, S.V., Lahmers, T.M., Liu, P.-W., Nie, W., Getirana, A.,  
759 Orland, E., Bindlish, R., Guzman, A., Hain, C.R., Melton, F.S., Locke, K.A., Yang, Y., 2024.  
760 Droughts impede water balance recovery from fires in the western United States. *Nat. Ecol.*  
761 *Evol.* 8, 229–238. <https://doi.org/10.1038/s41559-023-02266-8>.
- 762 Bär, A., Michaletz, S.T., Mayr, S., 2019. Fire effects on tree physiology. *New Phytol.* 223 (4),  
763 1728–1741. <https://doi.org/10.1111/nph.15871>.
- 764 Baur, M.J., Friend, A.D., Pellegrini, A.F.A., 2024. Widespread and systematic effects of fire on  
765 plant–soil water relations. *Nat. Geosci.* 17, 1115–1120.  
766 <https://doi.org/10.1038/s41561-024-01563-6>.
- 767 Beck, H. E., Zimmermann, N. E., McVicar, T. R., Vergopolan, N., Berg, A., Wood, E. F., 2018.  
768 Present and future Köppen-Geiger climate classification maps at 1-km resolution. *Scientific*  
769 *Data*, 5, 180214. <https://doi.org/10.1038/sdata.2018.214>.
- 770 Bernacchi, C.J., Kimball, B.A., Quarles, D.R., Long, S.P., Ort, D.R., 2007. Decreases in stomatal  
771 conductance of soybean under open-air elevation of [CO<sub>2</sub>] are closely coupled with decreases  
772 in ecosystem evapotranspiration. *Plant Physiol.* 143, 134–144.  
773 <https://doi.org/10.1104/pp.106.089557>.
- 774 Blanco-Rodríguez, M.Á., Ameztegui, A., Gelabert, P., Rodrigues, M., Coll, L., 2023. Short-term

775 recovery of post-fire vegetation is primarily limited by drought in Mediterranean forest  
776 ecosystems. *Fire Ecol.* 19, 68. <https://doi.org/10.1186/s42408-023-00228-w>.

777 Blunden, J., Arndt, D.S., 2012. State of the climate in 2011. *Bull. Am. Meteorol. Soc.* 93 (7), S1–  
778 S282. <https://doi.org/10.1175/2012BAMSStateoftheClimate.1>.

779 Boening, C., Willis, J.K., Landerer, F.W., Nerem, R.S., Fasullo, J., 2012. The 2011 La Niña: So  
780 strong, the oceans fell. *Geophys. Res. Lett.* 39 (19). <https://doi.org/10.1029/2012GL053055>.

781 Bonfils, C., Anderson, G., Santer, B.D., Phillips, T.J., Taylor, K.E., Cuntz, M., Zelinka, M.D.,  
782 Marvel, K., Cook, B.I., Cvijanovic, I., Durack, P.J., 2017. Competing influences of  
783 anthropogenic warming, ENSO, and plant physiology on future terrestrial aridity. *J. Clim.* 30  
784 (17), 6883–6904. <https://doi.org/10.1175/JCLI-D-17-0005.1>.

785 Chen, D., Fu, C., Jenkins, L.K., He, J., Wang, Z., Jandt, R.R., Frost, G.V., Bredder, A., Berner,  
786 L.T., Loboda, T., 2024. Regional fire–greening positive feedback loops in Alaskan Arctic  
787 tundra. *Nature Plants*. <https://doi.org/10.1038/s41477-024-01850-5>.

788 Chen, T., Guestrin, C., 2016. XGBoost: A scalable tree boosting system. In: *Proc. 22nd ACM*  
789 *SIGKDD Int. Conf. Knowl. Discov. Data Min.*, 785–794.  
790 <http://dx.doi.org/10.1145/2939672.2939785>.

791 Clarke, P.J., Lawes, M.J., Midgley, J.J., Lamont, B.B., Ojeda, F., Burrows, G.E., Enright, N.J.,  
792 Knox, K.J.E., 2013. Resprouting as a key functional trait: how buds, protection and resources  
793 drive persistence after fire. *New Phytol.* 197 (1), 19–35. <https://doi.org/10.1111/nph.12001>.

794 Cunningham, S.C., Read, J., 2003. Do temperate rainforest trees have a greater ability to acclimate  
795 to changing temperatures than tropical rainforest trees? *New Phytol.* 157(1), 55–64.  
796 <https://doi.org/10.1046/j.1469-8137.2003.00652.x>.

797 De Groot, W.J., Cantin, A.S., Flannigan, M.D., Soja, A.J., Gowman, L.M., Newbery, A., 2013. A  
798 comparison of Canadian and Russian boreal forest fire regimes. *For. Ecol. Manag.* 294, 23–  
799 34. <https://doi.org/10.1016/j.foreco.2012.07.033>.

800 Deng, Y., Li, X., Shi, F., Hu, X., 2021. Woody plant encroachment enhanced global vegetation  
801 greening and ecosystem water-use efficiency. *Glob. Ecol. Biogeogr.* 30 (12), 2337–2353.  
802 <https://doi.org/10.1111/geb.13386>.

803 Dukat, P., Kelly, J., Doerr, S.H., Edvardsson, J., Hött ä T.S., Lehner, I., Lindroth, A., Sant í, C.,  
804 Kljun, N., 2024. Boreal forest tree growth and sap flow after a low-severity wildfire. *Agric.*  
805 *For. Meteorol.* 347, 109899. <https://doi.org/10.1016/j.agrformet.2024.109899>.

806 Fan, S., Yang, Q., Li, S., Fristoe, T.S., Cadotte, M.W., Essl, F., Kreft, H., Pergl, J., Pyšek, P.,  
807 Weigelt, P., Kartesz, J., Nishino, M., Wieringa, J.J., van Kleunen, M., 2023. A latitudinal  
808 gradient in Darwin's naturalization conundrum at the global scale for flowering plants. *Nat.*  
809 *Commun.* 14(1), 6244. <https://doi.org/10.1038/s41467-023-41607-w>.

810 Farr, T.G., Rosen, P.A., Caro, E., Crippen, R., Duren, R., Hensley, S., Kobrick, M., Paller, M.,  
811 Rodriguez, E., Roth, L., Seal, D., Shaffer, S., Shimada, J., Umland, J., Werner, M., Oskin, M.,  
812 Burbank, D., Alsdorf, D., 2007. The Shuttle Radar Topography Mission. *Rev. Geophys.*  
813 45(2). <https://doi.org/10.1029/2005RG000183>.

814 Fernández-Guisuraga, J.M., Quintano, C., Fernández-Manso, A., Roberts, D.A., 2025. Biophysical  
815 drivers of short-term change in evapotranspiration after fire as estimated through the SSEBop  
816 Landsat-based model. *For. Ecol. Manag.* 594, 122945.  
817 <https://doi.org/10.1016/j.foreco.2025.122945>.

818 Friedl, M., Sulla-Menashe, D., 2022. MODIS/Terra+Aqua land cover type yearly L3 global 0.05 °  
819 CMG V061. Distributed by NASA EOSDIS Land Processes Distributed Active Archive  
820 Center. <https://doi.org/10.5067/MODIS/MCD12C1.061>.

821 Giglio, L., Justice, C., Boschetti, L., Roy, D., 2021. MODIS/Terra+Aqua burned area monthly L3  
822 global 500m SIN grid V061. Distributed by NASA EOSDIS Land Processes Distributed  
823 Active Archive Center. <https://doi.org/10.5067/MODIS/MCD64A1.061>.

824 Granged, A.J.P., Zavala, L.M., Jord án, A., B árcenas-Moreno, G., 2011. Post-fire evolution of soil  
825 properties and vegetation cover in a Mediterranean heathland after experimental burning: A  
826 3-year study. *Geoderma* 164, 85–94. <https://doi.org/10.1016/j.geoderma.2011.05.017>.

827 Ganjurjav, H., Hu, G., Zhang, Y., Gornish, E.S., Yu, T., Gao, Q., 2022. Warming tends to  
828 decrease ecosystem carbon and water use efficiency in dissimilar ways in an alpine meadow  
829 and a cultivated grassland in the Tibetan Plateau. *Agric. For. Meteorol.* 323, 109079.  
830 <https://doi.org/10.1016/j.agrformet.2022.109079>.

831 Greenwell, B.M., 2017. PDP: An R package for constructing partial dependence plots. *R J.* 9(1),  
832 421–436. <https://doi.org/10.32614/RJ-2017-016>.

833 Harris, I., Osborn, T.J., Jones, P., Lister, D., 2020. Version 4 of the CRU TS monthly  
834 high-resolution gridded multivariate climate dataset. *Sci. Data* 7(1), 109.  
835 <https://doi.org/10.1038/s41597-020-0453-3>.

836 He, N., Yin, J., Liu, P., Fu, X., Zhang, Q., Cheng, L., Moulds, S., Volchak, A., 2025. Global  
837 increases in dry–wet abrupt alternation events under climate change. *Geophys. Res. Lett.* 52  
838 (18), e2025GL117322. <https://doi.org/10.1029/2025GL117322>.

839 Hengl, T., Mendes de Jesus, J., Heuvelink, G.B.M., Ruiperez Gonzalez, M., Kilibarda, M.,  
840 Blagotić, A., Shangguan, W., Wright, M.N., Geng, X., Bauer-Marschallinger, B., Guevara,  
841 M.A., Vargas, R., MacMillan, R.A., Batjes, N.H., Leenaars, J.G.B., Ribeiro, E., Wheeler, I.,  
842 Mantel, S., Kempen, B., 2017. SoilGrids250m: Global gridded soil information based on  
843 machine learning. *PLOS ONE* 12(2), e0169748.  
844 <https://doi.org/10.1371/journal.pone.0169748>.

845 Hill, A.P., Field, C.B., 2021. Forest fires and climate-induced tree range shifts in the western US.  
846 *Nat. Commun.* 12, 6583. <https://doi.org/10.1038/s41467-021-26838-z>.

847 Hu, Z., Dai, Q., Li, H., Yan, Y., Zhang, Y., Yang, X., Zhang, X., Zhou, H., Yao, Y., 2024.  
848 Response of ecosystem water-use efficiency to global vegetation greening. *Catena* 239,  
849 107952. <https://doi.org/10.1016/j.catena.2024.107952>.

850 Huang, M., Piao, S., Sun, Y., Ciais, P., Cheng, L., Mao, J., Poulter, B., Shi, X., Zeng, Z., Wang,  
851 Y., 2015. Change in terrestrial ecosystem water-use efficiency over the last three decades.  
852 *Glob. Change Biol.* 21, 2366 – 2378. <https://doi.org/10.1111/gcb.12873>.

853 Hubbert, K.R., Wohlgemuth, P.M., Beyers, J.L., Narog, M.G., Gerrard, R., 2012. Post-fire soil  
854 water repellency, hydrologic response, and sediment yield compared between  
855 grass-converted and chaparral watersheds. *Fire Ecol.* 8, 143–162.  
856 <https://doi.org/10.4996/fireecology.0802143>.

857 Ito, A., Inatomi, M., 2012. Water-use efficiency of the terrestrial biosphere: A model analysis  
858 focusing on interactions between the global carbon and water cycles. *J. Hydrometeorol.* 13,  
859 681–694. <https://doi.org/10.1175/JHM-D-10-05034.1>.

860 Jin, J., Jian, D., Zhou, X., Chen, Q., Li, Y., 2025. Impact of El Niño–Southern Oscillation on  
861 global vegetation. *Atmosphere* 16 (6), 701. <https://doi.org/10.3390/atmos16060701>.

862 Jones, M.W., Abatzoglou, J.T., Veraverbeke, S., Andela, N., Lasslop, G., Forkel, M., Smith,  
863 A.J.P., Burton, C., Betts, R.A., van der Werf, G.R., Sitch, S., Canadell, J.G., Santín, C.,  
864 Kolden, C., Doerr, S.H., Le Quéré, C., 2022. Global and regional trends and drivers of fire  
865 under climate change. *Rev. Geophys.* 60 (3), e2020RG000726.  
866 <https://doi.org/10.1029/2020RG000726>.

867 Jung, M., Schwalm, C., Migliavacca, M., Walther, S., Camps-Valls, G., Koirala, S., Anthoni, P.,  
868 Besnard, S., Bodesheim, P., Carvalhais, N., Chevallier, F., Gans, F., Goll, D.S., Haverd, V.,  
869 Köhler, P., Ichii, K., Jain, A.K., Liu, J., Lombardozzi, D., Nabel, J.E.M.S., Nelson, J.A.,  
870 O'Sullivan, M., Pallandt, M., Papale, D., Peters, W., Pongratz, J., Rödenbeck, C., Sitch, S.,  
871 Tramontana, G., Walker, A., Weber, U., Reichstein, M., 2020. Scaling carbon fluxes from  
872 eddy covariance sites to globe: Synthesis and evaluation of the FLUXCOM approach.  
873 *Biogeosciences* 17, 1343–1365. <https://doi.org/10.5194/bg-17-1343-2020>.

874 Li, F., Xiao, J., Chen, J., Ballantyne, A., Jin, K., Li, B., Abraha, M., John, R., 2023. Global water  
875 use efficiency saturation due to increased vapor pressure deficit. *Science* 381, 672–677.  
876 <https://doi.org/10.1126/science.adf5041>.

877 Li, F., Xin, Q., Yi, C., Kannenberg, S.A., Green, J.K., Migliavacca, M., Moore, D.J.P., Kemanian,  
878 A.R., Gentine, P., Stoy, P.C., Zhang, F., Xiong, Y., Fu, Z., 2025. Limited regulation of  
879 canopy water use efficiency by stomatal behavior under drought propagation. *Glob. Change*  
880 *Biol.* 31 (7), e70381. <https://doi.org/10.1111/gcb.70381>.

881 Li, X., Xiao, J., 2019. Mapping photosynthesis solely from solar-induced chlorophyll fluorescence:  
882 A global, fine-resolution dataset of gross primary production derived from OCO-2. *Remote*  
883 *Sens.* 11, 2563. <https://doi.org/10.3390/rs11212563>.

884 Li, Y., Meng, L., Richardson, A.D., Lee, X., Menzel, A., Mao, J., Diehl, J.L., Wang, A., 2025.  
885 Cooling outweighs warming across phenological transitions in the Northern Hemisphere.  
886 *Proc. Natl. Acad. Sci. U.S.A.* 122 (37), e2501844122.  
887 <https://doi.org/10.1073/pnas.2501844122>.

888 Liu, S., Xue, L., Xiao, Y., Yang, M., Liu, Y., Han, Q., Ma, J., 2024. Dynamic process of  
889 ecosystem water use efficiency and response to drought in the Yellow River Basin, China.  
890 *Sci. Total Environ.* 934, 173339. <https://doi.org/10.1016/j.scitotenv.2024.173339>.

891 Liu, Z., Ballantyne, A.P., Cooper, L.A., 2019. Biophysical feedback of global forest fires on  
892 surface temperature. *Nat. Commun.* 10(1), 214. <https://doi.org/10.1038/s41467-018-08237-z>.

893 Lv, Q., Chen, Z., Wu, C., Peñuelas, J., Fan, L., Su, Y., Yang, Z., Li, M., Gao, B., Hu, J., Zhang, C.,  
894 Fu, Y., Wang, Q., 2025. Increasing severity of large-scale fires prolongs recovery time of  
895 forests globally since 2001. *Nat. Ecol. Evol.* 9, 980–992.  
896 <https://doi.org/10.1038/s41559-025-02683-x>.

897 Ma, N., Zhang, Y., 2022. Increasing Tibetan Plateau terrestrial evapotranspiration primarily driven  
898 by precipitation. *Agric. For. Meteorol.* 317, 108887.  
899 <https://doi.org/10.1016/j.agrformet.2022.108887>.

900 Madani, N., Parazoo, N.C., Kimball, J.S., Reichle, R.H., Chatterjee, A., Watts, J.D., Saatchi, S.,  
901 Liu, Z., Endsley, A., Tagesson, T., Rogers, B.M., Xu, L., Wang, J.A., Magney, T., Miller,  
902 C.E., 2021. The impacts of climate and wildfire on ecosystem gross primary productivity in  
903 Alaska. *J. Geophys. Res. Biogeosci.* 126 (6), e2020JG006078.  
904 <https://doi.org/10.1029/2020JG006078>.

905 Martin, K.C., Bruhn, D., Lovelock, C.E., Feller, I.C., Evans, J.R., Ball, M.C., 2010. Nitrogen  
906 fertilization enhances water-use efficiency in a saline environment. *Plant, Cell Environ.*  
907 33(3), 344–357. <https://doi.org/10.1111/j.1365-3040.2009.02072.x>.

908 McDowell, N.G., 2011. Mechanisms linking drought, hydraulics, carbon metabolism, and  
909 vegetation mortality. *Plant Physiol.* 155(3), 1051–1059.  
910 <https://doi.org/10.1104/pp.110.170704>.

911 Medlyn, B.E., De Kauwe, M.G., Lin, Y.-S., Knauer, J., Duursma, R.A., Williams, C.A., Arneeth,  
912 A., Clement, R., Isaac, P., Limousin, J.-M., Linderson, M.-L., Meir, P., Martin-StPaul, N.,  
913 Wingate, L., 2017. How do leaf and ecosystem measures of water-use efficiency compare?  
914 *New Phytol.* 216 (3), 758–770. <https://doi.org/10.1111/nph.14626>.

915 Mu, H., Li, X., Wen, Y., Huang, J., Du, P., Su, W., Miao, S., Geng, M., 2022. A global record of  
916 annual terrestrial human footprint dataset from 2000 to 2018. *Sci. Data* 9(1), 176.  
917 <https://doi.org/10.1038/s41597-022-01284-8>.

918 Muñoz Sabater, J., 2019. ERA5-Land monthly averaged data from 1981 to present. Copernicus  
919 Climate Change Service (C3S), Climate Data Store (CDS).  
920 <https://doi.org/10.24381/cds.68d2bb30>.

921 Myneni, R., Knyazikhin, Y., Park, T., 2021. MODIS/Terra+Aqua leaf area index/FPAR 4-day L4  
922 global 500m SIN grid V061. Distributed by NASA EOSDIS Land Processes Distributed  
923 Active Archive Center. <https://doi.org/10.5067/MODIS/MCD15A3H.061>.

924 NOAA National Weather Service, Climate Prediction Center, 2024. Cold & warm episodes by  
925 season: Oceanic Niño Index (ONI), version 5. Dataset.  
926 [https://origin.cpc.ncep.noaa.gov/products/analysis\\_monitoring/ensostuff/ONI\\_v5.php](https://origin.cpc.ncep.noaa.gov/products/analysis_monitoring/ensostuff/ONI_v5.php).

927 Nolan, R.H., Lane, P.N.J., Benyon, R.G., Bradstock, R.A., Mitchell, P.J., 2014. Changes in  
928 evapotranspiration following wildfire in resprouting eucalypt forests. *Ecohydrology* 7(5),  
929 1363–1377. <https://doi.org/10.1002/eco.1463>.

930 Paris, P., Di Matteo, G., Tarchi, M., Tosi, L., Spaccino, L., Lauteri, M., 2018. Precision subsurface  
931 drip irrigation increases yield while sustaining water-use efficiency in Mediterranean poplar  
932 bioenergy plantations. *Forest Ecol. Manag.* 409, 749–756.  
933 <https://doi.org/10.1016/j.foreco.2017.12.013>.

934 Poppe Ter an, C., Naz, B.S., Graf, A., Qu, Y., Hendricks Franssen, H.-J., Baatz, R., Ciais, P.,  
935 Vereecken, H., 2023. Rising water-use efficiency in European grasslands is driven by  
936 increased primary production. *Commun. Earth Environ.* 4(1), 95.  
937 <https://doi.org/10.1038/s43247-023-00757-x>.

938 Qiu, W., Zhao, Q., Yang, S., Xing, X., Azorin-Molina, C., Zhang, G., Zha, J., Deng, K., 2025.  
939 Relationship between different types of ENSO events and East Asian winter near-surface  
940 wind speed variability revealed by reanalyses and CMIP6 models. *Clim. Dyn.* 63 (10), 400.  
941 <https://doi.org/10.1007/s00382-025-07900-8>.

942 Ramo, R., Roteta, E., Bistinas, I., van Wees, D., Bastarrika, A., Chuvieco, E., van der Werf, G.R.,  
943 2021. African burned area and fire carbon emissions are strongly impacted by small fires  
944 undetected by coarse resolution satellite data. *Proc. Natl. Acad. Sci.* 118(9), e2011160118.  
945 <https://doi.org/10.1073/pnas.2011160118>.

946 Richardson, D., Black, A.S., Irving, D., Matear, R.J., Monselesan, D.P., Risbey, J.S., Squire, D.T.,  
947 Tozer, C.R., 2022. Global increase in wildfire potential from compound fire weather and  
948 drought. *npj Clim. Atmos. Sci.* 5, 23. <https://doi.org/10.1038/s41612-022-00248-4>.

949 Rogers, B.M., Soja, A.J., Goulden, M.L., Randerson, J.T., 2015. Influence of tree species on  
950 continental differences in boreal fires and climate feedbacks. *Nat. Geosci.* 8(3), 228–234.  
951 <https://doi.org/10.1038/ngeo2352>.

952 Sen, P.K., 1968. Estimates of the regression coefficient based on Kendall's tau. *J. Am. Stat. Assoc.*  
953 63(324), 1379–1389. <https://doi.org/10.1080/01621459.1968.10480934>.

954 Shakesby, R.A., Doerr, S.H., 2006. Wildfire as a hydrological and geomorphological agent.  
955 *Earth-Sci. Rev.* 74 (3–4), 269–307. <https://doi.org/10.1016/j.earscirev.2005.10.006>.

956 Skubel, R., Arain, M.A., Peichl, M., Brodeur, J.J., Khomik, M., Thorne, R., Trant, J., Kula, M.,  
957 2015. Age effects on the water-use efficiency and water-use dynamics of temperate pine  
958 plantation forests. *Hydrol. Process.* 29 (18), 4100–4113. <https://doi.org/10.1002/hyp.10549>.

959 Sperry, J.S., Love, D.M., 2015. What plant hydraulics can tell us about responses to climate -  
960 change droughts. *New Phytol.* 207(1), 14 - 27. <https://doi.org/10.1111/nph.13354>.

961 Sun, S., Xiang, W., Ouyang, S., Hu, Y., Peng, C., 2024. Balancing water yield and water use  
962 efficiency between planted and natural forests: A global analysis. *Glob. Change Biol.* 30 (11),  
963 e17561. <https://doi.org/10.1111/gcb.17561>.

964 Tang, X., Li, H., Desai, A.R., Nagy, Z., Luo, J., Kolb, T.E., Olioso, A., Xu, X., Yao, L., Kutsch,  
965 W., Pilegaard, K., Köstner, B., Ammann, C., 2014. How is water-use efficiency of terrestrial  
966 ecosystems distributed and changing on Earth? *Sci. Rep.* 4(1), 7483.  
967 <https://doi.org/10.1038/srep07483>.

968 Tang, X., Li, H., Ma, M., Yao, L., Peichl, M., Arain, A., Xu, X., Goulden, M., 2017. How do  
969 disturbances and climate effects on carbon and water fluxes differ between multi-aged and  
970 even-aged coniferous forests? *Sci. Total Environ.* 599, 1583–1597.  
971 <https://doi.org/10.1016/j.scitotenv.2017.05.119>.

972 Tangney, R., Miller, B.P., Fontaine, J.B., Merritt, D.J., Hobbs, R.J., Hardy, G.E.S.J., 2022.  
973 Success of post-fire plant recovery strategies varies with shifting fire seasonality. *Commun.*  
974 *Earth Environ.* 3, 245. <https://doi.org/10.1038/s43247-022-00453-2>.

975 Teskey, R., Wertin, T., Bauweraerts, I., Ameye, M., McGuire, M.A., Steppe, K., 2015. Responses  
976 of tree species to heat waves and extreme heat events. *Plant, Cell Environ.* 38(9), 1699–1712.  
977 <https://doi.org/10.1111/pce.12417>.

978 Tyukavina, A., Potapov, P., Hansen, M.C., Pickens, A.H., Stehman, S.V., Turubanova, S., Parker,  
979 D., Zalles, V., Lima, A., Kommareddy, I., Song, X.-P., Wang, L., Harris, N., 2022. Global  
980 trends of forest loss due to fire from 2001 to 2019. *Front. Remote Sens.* 3, 825190.  
981 <https://doi.org/10.3389/frsen.2022.825190>.

982 Valor, T., Casals, P., Altieri, S., González-Olabarria, J.R., Piqué M., Battipaglia, G., 2018.  
983 Disentangling the effects of crown scorch and competition release on the physiological and  
984 growth response of *Pinus halepensis* using  $\delta^{13}\text{C}$  and  $\delta^{18}\text{O}$  isotopes. *For. Ecol. Manag.* 424,  
985 276–287. <https://doi.org/10.1016/j.foreco.2018.04.056>.

986 Wang, J.A., Baccini, A., Farina, M., Randerson, J.T., Friedl, M.A., 2021. Disturbance suppresses  
987 the aboveground carbon sink in North American boreal forests. *Nat. Clim. Change* 11(5),  
988 435–441. <https://doi.org/10.1038/s41558-021-01027-4>.

989 Wand, S.J.E., Midgley, G.Y.F., Jones, M.H., Curtis, P.S., 1999. Responses of wild C4 and C3  
990 grass (Poaceae) species to elevated atmospheric CO<sub>2</sub> concentration: A meta - analytic test of  
991 current theories and perceptions. *Glob. Change Biol.* 5, 723–741.  
992 <https://doi.org/10.1046/j.1365-2486.1999.00265.x>.

993 Wang, Z., Fu, B., Wu, X., Li, Y., Feng, Y., Wang, S., Wei, F., Zhang, L., 2023. Vegetation  
994 resilience does not increase consistently with greening in China's Loess Plateau. *Commun.*  
995 *Earth Environ.* 4(1), 336. <https://doi.org/10.1038/s43247-023-01000-3>.

996 Wu, S., Li, D., Liu, L., Zhang, W., Liu, K., Zhao, W., Shen, J., Hao, C., Zhang, L., 2023. Global  
997 patterns and influencing factors of post-fire land cover change. *Global Planet. Change* 223,  
998 104076. <https://doi.org/10.1016/j.gloplacha.2023.104076>.

999 Xiao, J., Sun, G., Chen, J., Chen, H., Chen, S., Dong, G., Gao, S., Guo, H., Guo, J., Han, S., Kato,  
1000 T., Li, Y., Lin, G., Lu, W., Ma, M., McNulty, S., Shao, C., Wang, X., Xie, X., Zhang, X.,  
1001 Zhou, J., 2013. Carbon fluxes, evapotranspiration, and water use efficiency of terrestrial  
1002 ecosystems in China. *Agric. For. Meteorol.* 182, 76–90.  
1003 <https://doi.org/10.1016/j.agrformet.2013.08.007>.

1004 Xu, H., Chen, H.W., Chen, D., Wang, Y., Yue, X., He, B., Guo, L., Yuan, W., Zhong, Z., Huang,  
1005 L., Zheng, F., Li, T., He, X., 2024. Global patterns and drivers of post-fire vegetation  
1006 productivity recovery. *Nat. Geosci.* 17(9), 874–881.  
1007 <https://doi.org/10.1038/s41561-024-01520-3>.

1008 Xu, H., Xiao, J., Zhang, Z., Ollinger, S.V., Hollinger, D.Y., Pan, Y., Wan, J., 2020. Canopy  
1009 photosynthetic capacity drives contrasting age dynamics of resource use efficiencies between  
1010 mature temperate evergreen and deciduous forests. *Glob. Change Biol.* 26(11), 6156–6167.  
1011 <https://doi.org/10.1111/gcb.15312>.

1012 Xue, Y., Liang, H., Zhang, B., He, C., 2022. Vegetation restoration dominated the variation of  
1013 water use efficiency in China. *J. Hydrol.* 612, 128257.  
1014 <https://doi.org/10.1016/j.jhydrol.2022.128257>.

1015 Yao, Y., Liu, Y., Zhou, S., Song, J., Fu, B., 2023. Soil moisture determines the recovery time of  
1016 ecosystems from drought. *Glob. Change Biol.* 29(13), 3562–3574.  
1017 <https://doi.org/10.1111/gcb.16620>.

1018 Yang, S., Zhang, J., Zhang, S., Wang, J., Bai, Y., Yao, F., Guo, H., 2020. The potential of remote  
1019 sensing-based models on global water-use efficiency estimation: An evaluation and  
1020 intercomparison of an ecosystem model (BESS) and algorithm (MODIS) using site level and  
1021 upscaled eddy covariance data. *Agric. For. Meteorol.* 287, 107959.  
1022 <https://doi.org/10.1016/j.agrformet.2020.107959>.

1023 Yang, Y., Guan, H., Batelaan, O., McVicar, T.R., Long, D., Piao, S., Liang, W., Liu, B., Jin, Z.,  
1024 Simmons, C.T., 2016. Contrasting responses of water use efficiency to drought across global  
1025 terrestrial ecosystems. *Sci. Rep.* 6(1), 23284. <https://doi.org/10.1038/srep23284>.

1026 Yu, L., Fan, L., Ciais, P., Sitch, S., Fensholt, R., Xiao, X., Yuan, W., Chen, J., Zhang, Y., Wu, X.,  
1027 Qin, Y., Ma, M., Chang, Z., Wang, M., Yan, K., Song, L., Wigneron, J.-P., 2023. Carbon  
1028 dynamics of western North American boreal forests in response to stand-replacing  
1029 disturbances. *Int. J. Appl. Earth Obs. Geoinf.* 122, 103410.  
1030 <https://doi.org/10.1016/j.jag.2023.103410>.

1031 Yuan, W., Zheng, Y., Piao, S., Ciais, P., Lombardozzi, D., Wang, Y., Ryu, Y., Chen, G., Dong,  
1032 W., Hu, Z., Jain, A.K., Jiang, C., Kato, E., Li, S., Lienert, S., Liu, S., Nabel, J.E.M.S., Qin,  
1033 Z.C., Quine, T., Sitch, S., Smith, W.K., Wang, F., Wu, C., Xiao, Z., Yang, S., 2019.  
1034 Increased atmospheric vapor pressure deficit reduces global vegetation growth. *Sci. Adv.*  
1035 5(8), eaax1396. <https://doi.org/10.1126/sciadv.aax1396>.

1036 Yue, S., Pilon, P., Cavadias, G., 2002. Power of the Mann–Kendall and Spearman's rho tests for  
1037 detecting monotonic trends in hydrological series. *J. Hydrol.* 259(1–4), 254–271.  
1038 [https://doi.org/10.1016/S0022-1694\(01\)00594-7](https://doi.org/10.1016/S0022-1694(01)00594-7).

1039 Zhang, Y., Kong, D., Gan, R., Chiew, F.H.S., McVicar, T.R., Zhang, Q., Yang, Y., 2019. Coupled  
1040 estimation of 500 m and 8-day resolution global evapotranspiration and gross primary  
1041 production in 2002–2017. *Remote Sens. Environ.* 222, 165–182.  
1042 <https://doi.org/10.1016/j.rse.2018.12.031>.

1043 Zhang, Y., Wang, J.A., Berner, L.T., Goetz, S.J., Zhao, K., Liu, Y., 2024. Warming and  
1044 disturbances affect Arctic-boreal vegetation resilience across northwestern North America.  
1045 *Nat. Ecol. Evol.* 8, 2265–2276. <https://doi.org/10.1038/s41559-024-02551-0>.

1046 Zhang, Z., Zhang, L., Xu, H., Creed, I.F., Blanco, J.A., Wei, X., Sun, G., Asbjornsen, H., Bishop,  
1047 K., 2023. Forest water-use efficiency: Effects of climate change and management on the  
1048 coupling of carbon and water processes. *For. Ecol. Manag.* 534, 120853.  
1049 <https://doi.org/10.1016/j.foreco.2023.120853>.

1050 Zhao, A., Zhang, A., Cao, S., Feng, L., Pei, T., 2020. Spatiotemporal patterns of water use  
1051 efficiency in China and responses to multi-scale drought. *Theor. Appl. Climatol.* 140, 559–  
1052 570. <https://doi.org/10.1007/s00704-020-03103-9>.

1053 Zhao, J., Yue, C., Wang, J., Hantson, S., Wang, X., He, B., Li, G., Wang, L., Zhao, H., Luysaert,  
1054 S., 2024. Forest fire size amplifies postfire land surface warming. *Nature* 633, 828–834.  
1055 <https://doi.org/10.1038/s41586-024-07918-8>.